CONFORMATIONAL AND DYNAMICAL PROPERTIES OF HIGH PERFORMANCE POLYMERS DESIGNED FOR NOVEL APPLICATIONS

by

SERDAL KIRMIZIALTIN

Submitted to the Graduate School of Engineering and Natural Sciences
in partial fulfillment of
the requirements for the degree of
Master of Science

Sabancı University
Spring 2002

ABSTRACT

The conformational and dynamical properties of newly designed high performance polymers that may be utilized in a variety of industrial applications, are studied. In the first part, molecular dynamics simulations under different conditions and Rotational Isomeric States calculations are performed to understand the local and global conformational properties of the bacterial polyester, poly(3-hydroxyundecanoate). The rotational isomeric state model is incorporated with Monte Carlo simulations to calculate the dimensions and the characteristic ratio of the infinitely long chain. These calculations, performed in vacuum, predict a Gaussian distribution for the end-to-end vector with a non-zero mean and a value of 5.5 for the characteristic ratio. Molecular dynamics simulations predict the characteristic ratio of the single chain in good solvent, and of chains in the bulk state as 23 and 18, respectively. The role of temperature on the overall dimensions and on the distribution of dihedral angles is discussed. Radii of gyration and helix formation propensities at different temperatures and in different media are compared. The chain in solution is found to have the largest persistence length with the highest helical persistence. Results are compared with experimental and theoretical studies conducted on poly(3-hydroxybutyrate), which has the same backbone structure, but a different type of side-chain.

In the second part, novel block co-oligomers are designed as candidate surfactants in near supercritical CO_2 environment, with the CO_2 – phobic block consisting of ethyl propionate and 10 different types of ethylene monomers, flanked on either side by eight repeat unit fluorinated CO_2 – philic blocks. Single chain molecular dynamics simulations are performed to understand their conformational and dynamic properties. Depending on the side chain type, the CO_2 – phobic blocks are prone to shrinkage in the CO_2 environment, while the CO_2 – philic blocks preserve their vacuum dimensions. The overall chains form U-shaped planar structures with flapping motion of the fluorinated

arms; thus, we expect bilayer micelle formation under these conditions. The origin of the CO_2 – oligomer interactions are investigated and van der Waals interactions are found to dominate over electrostatic interactions in the CO_2 environment. Calculations of the radial distribution function for the solvent molecules around the oligomer backbone show a solvation shell around 5 - 6 Å, irrespective of the oligomer type; density of the solvent around the oligomer, on the other hand, varies with type of side chain due to the interactions between the CO_2 molecules and the oligomer, and the available volume around the side chain. The local chain dynamics are investigated by orientational autocorrelation functions, and the characteristic time of the relaxation of selected C-H and C-F bonds is found to depend on the local friction experienced by the fluctuating atoms and the energy barrier that needs to be surmounted during the relaxation process. The simple exponential decay of the correlation functions for the C-H bond is common for all oligomer types, whereas the stretched exponents take on smaller values depending on the side chain for the C-F bond vector, implicating that the fluorinated blocks are exposed to more complicated dynamical processes.

ÖZET

Birçok endüstriyel uygulamarı olası yüksek performanslı yeni tasarım polimerlerin konformasyonel ve dinamik özellikleri incelenmiştir. Birinci bölümde bakteriel poliester çeşidi poli(3-hidroksiundekanoatin)'in lokal ve global konformasyonel özelliklerini anlamak amacıyla farklı şartlarda moleküler dinamik simülasyonları ve Dönme Izomerleri Modeli hesaplamarı yapılmıştır. Sonsuz uzunluktaki zincirin boyutları ve karakteristik oranını hesaplamak için Monte Carlo simülasyonları içeren Dönme Izomerleri Modeli kullanılmıştır. Vakum ortamında yapılan bu hesaplamalar, iki uç arasındaki vektör için sıfırdan farklı bir ortalamaya sahip Gaussian dağılımı ve karakterisitik oranı için 5.5 sonucunu öngörmüştür. Moleküler dinamik simülasyonları iyi çözücüdeki tek zincirin ve amorf durumdaki zincirlerin karakteristik oranını sırasıyla 23 ve 18 olarak öngörmüştür. Sıcaklığın genel boyut ve dönme açıları üzerindeki etkisi ele alınmıştır. Farklı sıcaklık ve ortamlarda dönme yarıçapı ve heliks oluşma eğilimleri karşılaştırılmıştır. Çözelti içindeki zincirin en yüksek kalıcı uzunluk ve en yüksek heliks bulundurma oranına sahip olduğu bulunmuştur. Sonuçlar omuga yapısı aynı, yan zincirleri farklı olan poli(3-hidroksibutirat) konusunda yapılan deneysel ve teorik çalışmalarla karşılaştırılmıştır.

İkinci bölümde, süperkritik CO_2'ye yakın ortamda sürfaktan adayı, etil propionat ve 10 farklı tip etilen monomer içeren CO_2 – fobik blok ile her iki yanında sekizer monomer birimi florokarbon içeren CO_2 – filik bloktan oluşan yeni blok ko-oligomerler dizayn edilmiştir. Konformasyonel ve dinamik özelliklerini anlamak için tek zincir moleküler dinamik simülasyonları yapılmıştır. Yan zincir tipine bağlı olarak CO_2 ortamında CO_2 – fobik bloklar büzülme eğilimi gösterirken, CO_2 – filik kısımlar vakum boyutlarını korumuştur. Zincirler florlu kolları açılıp kapanan U-şeklinde düzlemsel yapılar oluşturmuşlardır; bu nedenle bu şartlarda çift katmanlı misel oluşumu beklenmektedir. CO_2 ortamında CO_2 – oligomer etkileşimlerinin kökeni araştırılmıştır

ve van der Waals etkileşimlerinin elektrostatik etkileşimlere baskın olduğu bulunmuştur. Oligomer omurgasının etrafındaki çözücü moleküllerin radyal dağılım fonksiyonu oligomer tipinden bağımsız olarak 5 - 6 Å aralığında bir çözülme kabuğu göstermiştir. Oligomerlerin etrafındaki yoğunluk, diğer yandan, CO_2 molekülleri ile etkileşimler ve yan zincirler etrafındaki mevcut hacim nedeniyle değişiklik göstermiştir. Yerel zincir dinamiği oryantasyonel otokorelasyon fonksiyonu ile incelenmiş, ve belirli C-H ile C-F bağlarının gevşeme karakteristik zamanının salınan atomların maruz kaldığı yerel sürtünme ve gevşeme sürecinde etkin olan enerji engelinin aşılmasına bağlı olduğu bulunmuştur. Tüm oligomer tiplerinin C-H bağlarının korelasyon fonksiyonları için basit üstel bozunma ortak özellikken, yan zincire bağlı olarak C-F bağ vektörü daha küçük üstel değerler aldı, bu da florlu bloğun daha karmaşık dinamik süreçlere maruz olduğunu göstermektedir.

ACKNOWLEDGEMENTS

TABLE OF CONTENTS

LIST OF TABLES

x

LIST OF FIGURES

LIST OF SYMBOLS

Å	Angstrom
$A_{3xn}(j)$	transpose of x, y, z components of the jth configuration
$C_i(t)$	orientational autocorrelation function for a given bond i
C_n	characteristic ratio of n number of bonds
C_∞	characteristic ratio for infinitely long chain
$E_{CO2/CO2}$	solvent–solvent interactions
E_{mxm}	identity matrix of order m
ΔE_{mix}	change in the internal energy of system due to mixing
E_{nb}	nonbonded energy including both oligomer and solvent
$E_{O/CO2}$	oligomer–solvent interactions
$E_{O/O}$	oligomer–oligomer interactions,
ΔF_{mix}	Helmholtz free energy of system due to mixing
$g^\pm$	gauche$^+$ and gauche$^-$ conformer of dihedral angles
g_{ab}	radial distribution function of a around b
l	bond length
$l^{'}$	Kuhn length
l_p	persistence length
M	molar mass
m_i	mass of the ith atom
n	number of bonds
N	number of repeat units
$n^{'}$	number of Kuhn segments
$P(\omega,\varphi)$	probability of having ω, φ rotational pairs
p_i	contribution fraction of a vector to the overall shape
r	end-to-end distance

-R	functional group
$\langle r \rangle$	average end-to-end distance
$\langle r^2 \rangle_o$	average root mean square end-to-end distance in unperturbed state
r_{ab}	distance between centers of atoms a and b
r_{cm}	position vector of the center of mass relative to a fixed frame
R_g	radius of gyration of the backbone
r_i	position vector of the ith atom relative to a fixed frame
r_{max}	maximum end-to-end distance
ΔS_{mix}	change in entropy of system due to mixing
t	trans conformer of dihedral angles
U_{3x3}	left singular matrix of the decompositon of A_{3xn}
u_i	left singular vectors of A
$u_i(t_o)$	unit vector of the ith bond at time t_o
$u_i(t+ t_o)$	unit vector of the ith bond with a time delay of t
$U(r_1, r_2, ..., r_N)$	potential energy as a function of atomic positions
V_{3xn}	right singular matrix of decomposition of A_{3xn}
v_i	right singular vector
$W(r)$	spatial distribution of end-to-end distance
w_i	singular values of A
β	stretch exponent of Kohlrausch-Williams-Watts function
γ	relative population of the rotamers
δ_{ij}	Kronecker delta
$\omega, \varphi, \phi, \chi$	internal rotational angles of the backbone
σ	standard deviation
$\langle \rho_a \rangle$	average number density of a
ρ	number density of the system
ρ_{ab}	number density of finding particle a around b
τ_i	characteristic time for the relaxation of bond i

LIST OF ABBREVIATIONS

CFF91	Consistent Forcefield 91
CVFF	Consistent Valence Forcefield
MC	Monte Carlo
MD	Molecular Dynamics
NMR	Nuclear Magnetic Resonance
NVT	Canonical Ensemble
OACF	Orientational Auto Correlation Function
ORD	Optical Rotatory Dispersion
PBC	Periodic Boundary Conditions
PCFF	Polymer Consistent Forcefield
PET	Polyethylene terephtylate
PHA	Poly Hydroxy Alkanoate
PHB	Poly(3-hydroxybutyrate)
PHU	Poly(3-hydroxyundecanoate)
RDF	Radial Distribution Function
RIS	Rotational Isomeric State
SANS	Small Angle Neutron Scattering
SAXS	Synchrotron small Angle X-ray Scattering
TFE	2,2,2-trifluoroethanol

1. INTRODUCTION

A polymer is a macromolecule that is constructed from chemically linked sequences of molecular fragments[1]. For synthetic polymers, these fragments comprise the same basic unit called repeat unit. The large variety of chemical constitution and the specific molecular architecture of the repeat units are responsible for the wide range of properties that the polymeric materials show. Even in the same chemical constitution, different conformational properties are observed depending on the environment and other thermodynamic conditions such as temperature and pressure. In good solvents, the intra-chain repulsion or excluded volume between the segments expands the polymer dimensions, as does the solvent-solute interactions. In less favorable solvents, however, the solvent-solute and solute-solute interactions have opposite signs, and when they are precisely balanced, the chain dimensions are independent of both segment-segment and solvent-solute interactions. This phenomenon occurs at a particular temperature/solvent combination, where chain dimensions correspond to the dimension of a volumeless non-interacting (i.e. unperturbed) polymer coil. In the poor solvent regime, on the other hand, the attractive and repulsive forces are no longer balanced, and solute-solute interactions cause chain dimensions to dramatically decrease, hence the polymer chain collapses[2].

Due to their large number of atoms bonded together forming a long chain, polymers can generally adopt a multitude of conformations. These conformations arise from the numerous internal rotations, originating from a number of rotational isomers. Nevertheless, although the rotation around each bond is able to generate different conformations, due to energy restrictions not all of them have the same probability of occurrence. Under these circumstances, the most stable conformations predominate in solution; such behavior is observed mainly in biopolymers. However, synthetic polymers can display a large number of possible conformations, and even though these

conformations do not have the same energy, the differences are small enough so that the chains can change from one conformation to another, forming a random coil. In very dilute solutions, the average distances between dissolved molecules are rather large. Therefore, the intermolecular interactions may be neglected and the properties of single (isolated) molecules should suffice to describe such systems.

Polymers are dynamic moieties, the fastest motions in a polymeric system is the chemical bond stretching vibration which is typically occurring on the order of 10 fs whereas, some collective phenomena such as dissolving a polymer in solution and protein folding may take seconds[1, 3]. The size scale, on the other hand, ranges from 1-2 Å of chemical bonds to the diameter of a coiled polymer that can be several hundred angstroms[4]. Long-time and long-length scale modelling, which is often necessary to track the dynamical and morphological characteristics of polymeric systems, is a great challenge in polymer simulations.

When the prediction of a real polymer behavior is aimed, molecular models with different levels of complexity have been employed. The approaches developed to understand the problems are by necessity coarse-graining where detailed chemical specificities are not taken into account. Despite the lack of details, these models can predict many physical properties of polymers such as rubber elasticity, molecular shapes of polymer coils in dilute regime, etc. However, coarse-grained approaches in general are not adequate to investigate the properties which are affected by the intrinsic conformational features of the chains, such as the local chain properties of polymers that have large side groups[5].

The molecular dynamics (MD) method, where full atomistic descriptions of atoms are explicitly considered, can be effectively utilized to understand the behavior of small oligomers at the molecular level and to design high performance materials. Among these oligomers, amphiphilic molecules such as lipids and surfactants, that contain a hydrophobic head and a hydrophilic tail have great importance for industrial applications and biological processes[6]. These are capable of forming a variety of complex structures including micelles, vesicles, bilayers and liquid crystalline structures depending on the molecular architecture and the thermodynamic conditions of the environment.

In this thesis, the conformational and dynamical properties of newly designed high performance polymers that may be utilized in a variety of industrial applications, is studied. In the first part, the isolated chains and bulk properties of a particular

biopolyester iso-poly(3-hydroxundecanoate) in the poor, theta, and good solvent regimes are investigated. The chain dimensions calculated by Rotational Isomeric State (RIS) model are compared with chain dimensions predicted by MD methods; helix formation propensities at different temperatures and in different environments are compared. In the second part, conformational features of novel surfactant amphiphiles designed for supercritical CO_2 applications are examined. Local and global structures of the CO_2 - philic and CO_2 - phobic blocks are analysed. The energetics of solvation, the organization of the solvent around the surfactants and the local dynamics of the chains are investigated.

2. CONFORMATIONAL PROPERTIES OF THE BACTERIAL POLYESTER POLY(3-HYDROXYUNDECANOATE) IN DIFFERENT TEMPERATURES AND AT DIFFERENT ENVIRONMENTS

2.1. Overview

Bacterial polyesters are naturally occurring polymers, which act as important storage materials in a variety of bacteria. Elementary analysis, infrared spectroscopy, autolysis, saponification and degradation experiments all support a linear head-to-tail polyester structure with the general formula[7],

$$-O-C(HR_1)-C(R_2R_3)-CO-$$
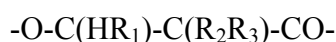
where R_1, R_2 and R_3 are the side groups. The functional units of the above polyesters, which have the generic name of polyhydroxy alkanoates (PHAs), are determined by the bacterial species and feedstock. By this means, PHAs with improved physical features can be produced. These polymers (i) are biodegradable in water and carbon dioxide[8], (ii) are thermoplastic, and (iii) act as a carbon and energy reserve[9]. Therefore, they are foreseen as clean alternatives of many industrially important polymers such as polypropylene. However, they are unstable at processing temperatures, and have poor mechanical properties for industrial applications. To remedy these problems, copolymers of certain biopolyesters have been synthesized. For example, poly(3-hydroxybutyrate-co-3-hydroxyvalerite), Biopol®, has achieved a limited industrial application[8, 9].

Among the large class of biopolyesters, the conformational properties and local chain dimensions in different environments of poly(3-hydroxybutyrate), PHB, have been extensively studied. The solid state properties of PHB was first studied by Cornibert et al.[7] Their x-ray analysis showed that PHB crystallizes into a left-handed

2_1-helix with two unparallel chains packed in an orthorhombic unit cell. These authors have proposed that the backbone dihedrals have repeated stretches of the states ttg^+g^+, where g^+ is approximately perpendicular to the fibre axis. The ester bond, on the other hand, was observed to have a small deviation from planarity. They reported the angle between the dipoles of the ester groups as ~60° in the unit cell and suggested that dipole-dipole interactions were the main factor determining the packing and the overall conformation.

Brückner et al. [10] undertook both isotactic and lower tacticity racemic polymers of PHB and observed similar results with the previous study with an extra refinement of the unit cell parameters. In another study, Pazur and coworkers[9] have employed molecular modelling and x-ray fibre diffraction techniques to investigate the crystalline chain conformations of a series of PHBs. Among the minimum energy conformations, a left-handed 2_1 helix with lattice parameters similar to the X-ray data of Brückner's study was reported for the iso-PHB.

Solution properties of PHB were studied by intrinsic viscosity, sedimentation analysis and optical rotatory dispersion experiments (ORD) by Marchessault and Okamura[11]. Viscometry and ORD experiments performed in chloroform indicated partially rodlike linear chains. The chain size was found to have a minor effect on the conformation. Depending on the solvent type and temperature, either randomly coiled or partially helical segments were proposed. As the solvent composition and temperature changed, a sharp helix-coil transition similar to that observed in proteins occurred. Einaga and coworkers[12] subsequently studied the dilute solution properties of a series of fractionated PHBs by light scattering and viscosity experiments. While they were unable to reproduce the ORD observations of Marchessault and Okamura, which had suggested a propensity to the helices in some solutions. Instead, they reported a randomly coiling structure in dilute solution of good solvents such as 2,2,2-trifluoroethanol (TFE). In addition, when their data extrapolated to the unperturbed state C_∞ is found as ca. 8.

The unperturbed dimensions of PHB in the non–solvent TFE/water was studied by Huglin et al. [13] They reported unperturbed dimensions, $(<r^2>_0/M)^{1/2}$, as 0.085 nmg$^{-1/2}$mol$^{1/2}$ where, $<r^2>_0$ is the mean-square end-to-end distance and M is the molar mass. If the average bond length square ($<l^2>$) is taken as 2.07 Å^2 and molecular weight of 86 gr/mol then C_∞ is calculated as ca. 7.5 from these experiments. Beaucage et al. [14], on

the other hand, observed high degree of local chain persistence and unusual rheology for iso-PHB in the amorphous state. The C_∞ in the amorphous state was found to be ca. 40 from the persistence length measurements using both small angle neutron scattering (SANS) and rheology experiments. The studies reviewed above reveals that experimental results are open to interpretations and there are controversies about the chain dimensions in the unperturbed state, and existence of helical segments in solution. A detailed analysis of conformational properties will lead to a better understanding of these experiments.

One of the few studies of the conformational properties of PHAs is by Marchessault and collaborators[9]. In their molecular mechanics study, helical propensities of PHB as well as other short side-group PHAs such as poly(3-hydroxybutyrate-c-3-hydroxyvalerate), poly(4-hydroxybutyrate), and poly(tetramethyl-enesuccinate) were determined. Results showed a strong tendency to form helical structures in the minimum energy conformation. This was also verified by experiments[11]. These chains exhibit various degrees and types of crystallinity in the bulk state depending on their chemical identity and the type and location of their side groups.

2.2. Molecular Model and Computational Methods

We study the conformational characteristics of a different class of PHA, namely poly(3-hydroxyundecanoate) (PHU), where the side groups R_2 and R_3 are hydrogens and R_1 is an aliphatic long chain, $CH_2 - (CH)_2 - CH_2 - (CH)_2 - CH_3$ (cf Figure 2.1). The relatively large size and flexibility of the side groups introduce significant entropic effects to the statistics of these chains. Due to their large sizes, the side chains also cause considerable crowding. Hence the conformational features of these molecules are expected to differ significantly, especially with regard to unperturbed dimensions and helical propensities, from those of the PHBs studied earlier. In the interest of understanding the statistical properties of these chains in different thermodynamic conditions, RIS model and MD methods are performed. Results are compared with the experimental and theoretical studies performed for the PHBs.

2.2.1. Unperturbed State and Rotational Isomeric States Model

The dimension of a single chain depends on the short-range and long-range interactions between the chain segments. The short-range interactions are bonded interactions that depend on the deviations of the chemical bond lengths, bond angles and dihedral angles from their equilibrium values and local non-bonded interactions, which are near-neighbor in sequence along the chain. The long-range interactions, on the other hand, involve non-bonded interactions between pairs, which are remote in the chain sequence but near to one another in space. The unperturbed state is the particular
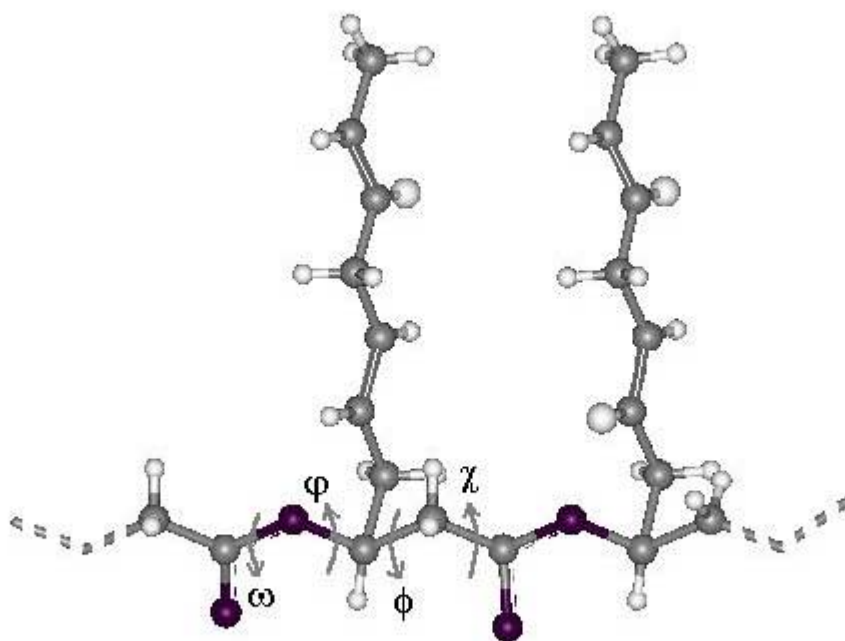
Figure 2.1. Two repeat units of the aliphatic polyester isotactic PHU with the bulky side chains of CH_2 - $(CH)_2$ - CH_2 - $(CH)_2$ - CH_3. The ω, φ, ϕ, χ denote the internal rotational angles of the backbone.

state in which the molecule is subject to the local constraints relating to the geometrical features of the bond structure and the hindrances to rotation about bonds i.e. it is the state where short-range interactions are considered only. For that reason, the

unperturbed state is assumed as the reference state in which the molecule is free of non-local constraints.

The polymer chains have hindrances that restrict their rotation to a small number of rotations called rotational states. The numeric method of analyising the chain statistics considering these discrete rotatamers is called the Rotational Isomeric States model. To a good degree of approximation, only the interactions between the nearest-neighbor bonds are considered and higher order interactions are ignored in rotational energy calculations. The bond lengths and valence angles are held fixed at the equilibrium values for convenience. If the relative conformational energies of these states are known, the relative population of the rotamers, γ, can be calculated with the Boltzmann weight formula as $\gamma = \exp[-E(\theta_1,\theta_2)/RT]$ where $E(\theta_1,\theta_2)$ represents the energy as a function of the rotational angle pair (θ_1, θ_2). The conformation of a chain having n bonds is represented by statistically weighted rotational states generated by Monte Carlo chain generation technique and the matrix multiplication methods given in Reference[15]. The chains generated by this way have the properties of unperturbed chains, and their conformations remain unaffected by the non-local interactions such as excluded volume effect.

To perform RIS calculations, the dimer molecule of the PHU was energy minimised using the Polymer Consistent Forcefield (PCFF)[16, 17] implemented within the Molecular Simulations Inc. InsightII 98.0 software package, with a stringent minimization criterion of at least 10^{-3} kcal/mol/Å of the derivative. During torsional angle variations, the valence angles and bond lengths were assumed to be fixed at the equilibrium bond lengths and valence angles of the minimized geometry. Long-range interactions were ignored by considering only the non-bonded contributions from near neighbors. Thus, the conformation of the chain was described by four torsional angles ω, φ, ϕ, χ for the RIS model. The rigid rotor approximation was used for the rotatable bonds and fluctuations in the bond stretching and bending were ignored. The energies corresponding to the three rotational pairs i.e. (ω, φ), (φ, ϕ) and (ϕ, χ), were calculated by 1° increments of the torsional angles. Energy calculations were performed with no minimization and no distance cut-off.

2.2.2. Molecular Dynamics Simulation Method

In the MD simulations, the chain dimensions can be calculated by solving the Newton's equation of motion for each of the particle explicitly with the formula:

$$m_i \frac{d^2 r_i(t)}{dt^2} = -\frac{\partial}{\partial r_i} U(r_1, r_2, ..., r_N) \qquad i = 1, ..., N \quad (2.1)$$

Here N is the number of atoms in the system, m_i and r_i are the mass and position of particle i. $U(r_1, r_2, ..., r_N)$ is the potential energy as a function of atomic positions and is generally called forcefield. The Polymer Consistent Forcefield (PCFF)[16, 17] used in this chapter consists of bonded and nonbonded types of interactions for the polymeric systems that is parameterized by semi-empirical and ab-initio quantum mechanical calculations as well as experiments.

We carried out MD simulations in vacuum, in the bulk and in chloroform solution, treating all atoms explicitly. The PHU system utilized in the simulations consists of 30 monomer units and has an initially extended structure with an end-to-end distance of ca. 122 Å. A time step of 0.5 fs was used, and the temperature was kept fixed at the desired value by using the temperature control method of Andersen[18, 19]. Initial velocities were generated from a Boltzmann distribution and integration was carried out by the Velocity Verlet algorithm[20]. Group-based cutoffs were used with a 9.5 Å cutoff distance; a switching function was used with the spline and buffer widths set to 1.0 and 0.5 Å, respectively. The neighbour list was updated whenever any atom moved more than one-half the buffer width. The PCFF parameters were used for energy calculation. The positions of atoms were recorded every 2 ps for further analysis. In the first part of the MD calculations, behaviour of the single chain in vacuum at the temperatures of 250, 300, 350 and 400 K were analyzed. All of the geometries were optimized by the Conjugate Gradients method up to a final convergence of 0.1 kcal/mol/Å. After generation and minimization of all the systems, dynamic calculations were performed with 50 ps equilibration followed by a 1.0 ns data collection stage.

For the bulk simulations, five initially extended chain molecules were placed in a box with $25 \times 25 \times 120$ Å^3 dimensions, corresponding to a density of 0.56 g/cm^3. Periodic Boundary Conditions (PBC) were applied with a cut-off radius of 9.5 Å for all

nonbonded interactions and van der Waals tail corrections were taken into account[20]. The initially packed cell was optimized by first the Steepest Descents and then Conjugate Gradients methods up to a final convergence of 0.05 kcal/mol/Å of the derivative. To remove bad contacts, the system was refined by an NVT simulation at 300 K, where the temperature was controlled for 0.1 ns by velocity rescaling followed by 0.4 ns of Nosé protocol[21]. After equilibration was reached, 1.1 ns of MD simulation was performed with the Andersen temperature control method at the same temperature.

For the simulation in solvent, one single chain of PHU was immersed in a cubic box of 52 Å dimensions with 1000 chloroform (CH_3Cl) molecules in it. This corresponds to a density of 1.49 g/cm^3, which is the experimentally measured density of chloroform. The other simulation details are the same for the simulations in bulk. In all simulations, the various quantities investigated were calculated from the portion of the MD trajectories for which equilibrium has been reached.

2.3. Results and Discussion

2.3.1. RIS Model Results

2.3.1.1. Statistical Weight Matrices for Interdependent Bonds

The overall dimensions of a chain depend strongly on the conformation of the backbone atoms. The backbone of the PHU molecule has four bond vectors. The partial double bond nature of the ester bond, shown in Figure 2.1, restricts the rotation angle ω to the trans state (0° in Flory representation, Reference[15]). We carried out single point energy calculations for every increment of rotation between the pairs (ω, φ), (φ, ϕ) and (ϕ, χ) as labelled in Figure 2.1. The results of conformational energy calculations corresponding to three rotational bond pairs (ω, φ), (φ, ϕ) and (ϕ, χ) are given in Figures 2.2-2.4.
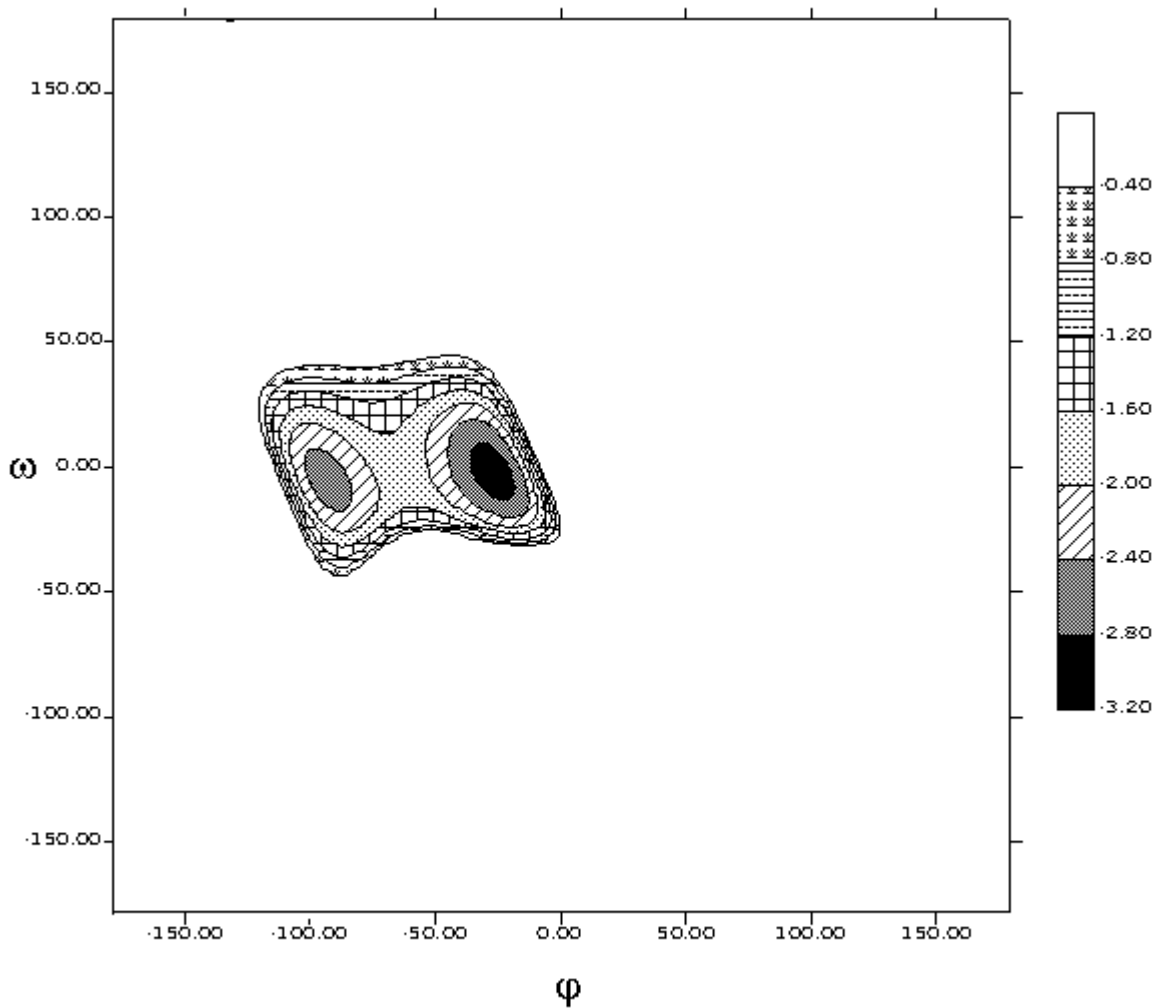
Figure 2.2. Energy contour map of the ω, φ rotation pairs in kcal/mole. The energy values greater than -0.4 kcal/mole are not shown for convenience. The minima for the ω, φ rotations are *tt* and *tg⁻*

The torsional states *t, g⁻* and *g⁺* for each bond were obtained from the energy surfaces expressed in terms of torsional angle pairs, similar to the polyethylene model. The rotational minima for the three states *t, g⁻* and *g⁺* exhibited shifts of ± 20 from the ideal *gauche* and *trans* values. In particular, the *trans* state of the φ torsion occurs at $40 \pm 10°$. The statistical weight matrices constructed for the RIS model at 300 K from the conformational energies are as follows:
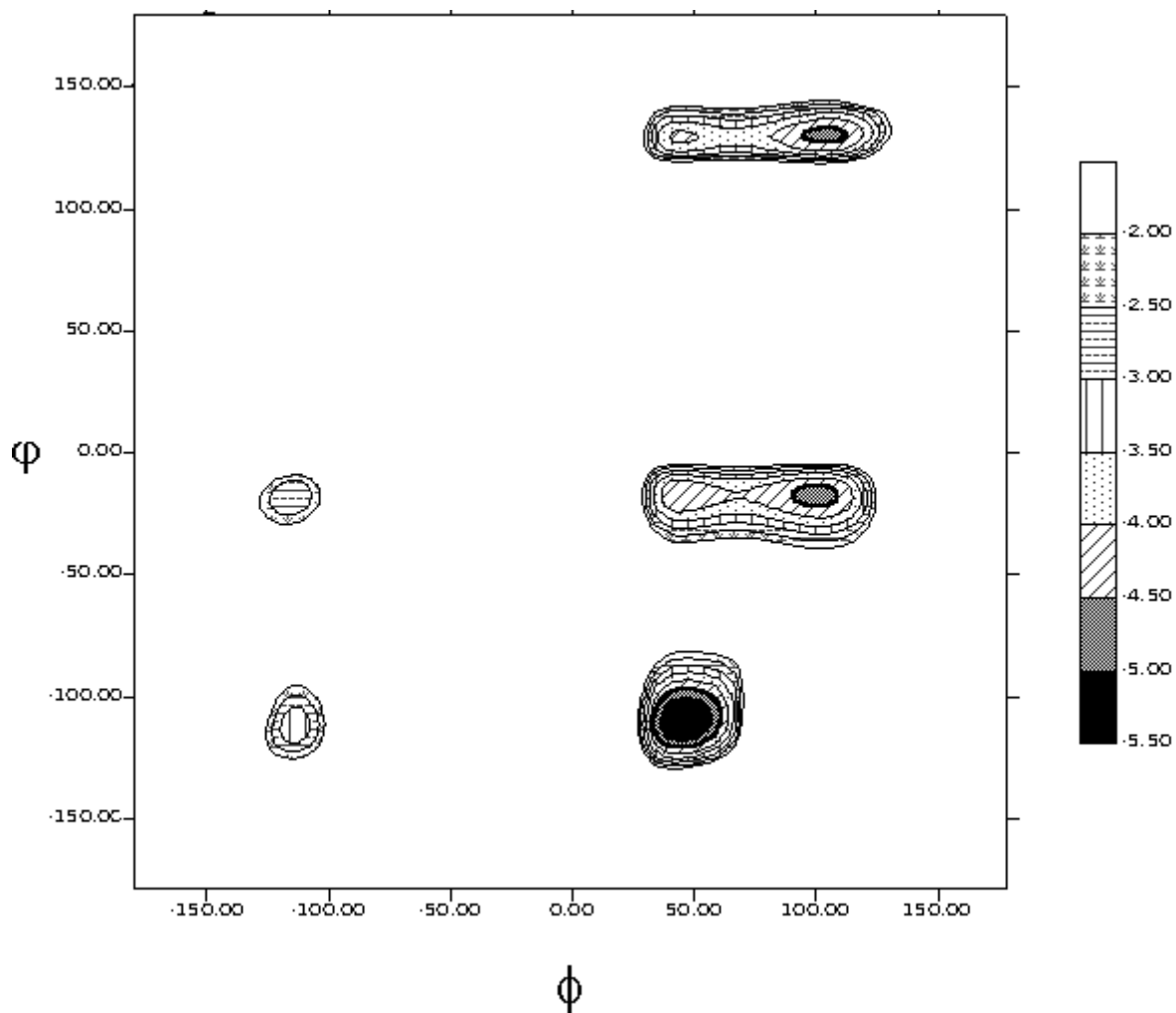
Figure 2.3. Energy contour map of the φ, ϕ rotation pairs in kcal/mole. The energies greater than −2.0 kcal/mole are not shown for convenience. The minima for the φ, ϕ pairs occur at g^-t, gt^+

$$P(\omega,\varphi) = \begin{array}{ccc} t & g^- & g^+ \end{array}$$
$$P(\omega,\varphi) = [\ 0.7320\ \ 0.0005\ \ 0.2675]$$

$$
P(\varphi,\phi) =
\begin{array}{ccc}
t & g^- & g^+
\end{array}
\begin{bmatrix}
0.1276 & 0.2496 & 0.0912 \\
0.0238 & 0.0086 & 0.0000 \\
0.2496 & 0.2496 & 0.0000
\end{bmatrix}
$$
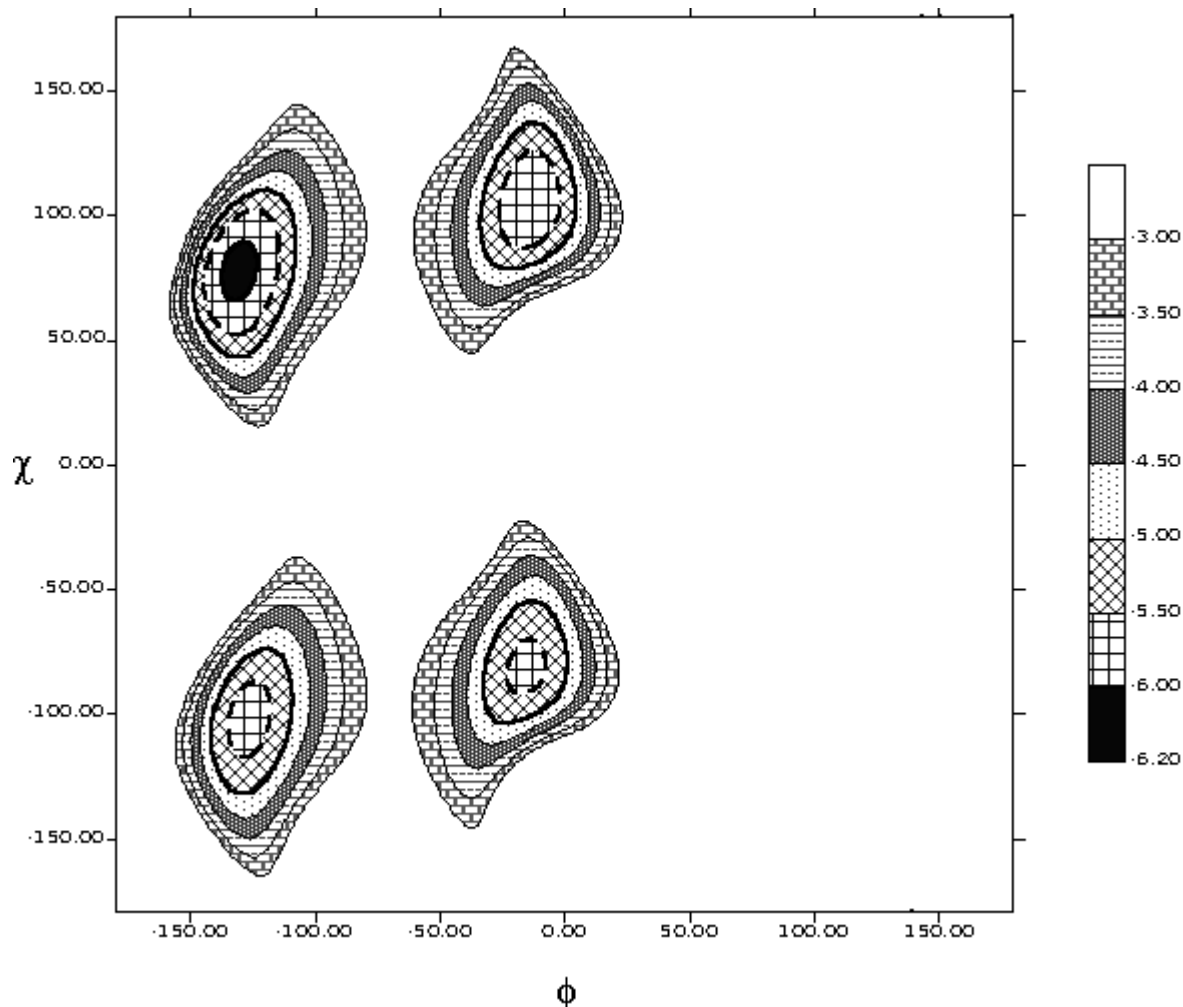
Figure 2.4. Energy contour map of the χ, ϕ rotation pairs in kcal/mole. The energies greater than -3.0 kcal/mole are not shown for convenience. The minimum for the χ, ϕ pairs occur at g^+g-.

$$
\begin{array}{ccc}
t & g^- & g^+ \\
\end{array}
$$
$$
\begin{bmatrix}
0.0000 & 0.1630 & 0.2280 \\
0.0000 & 0.1630 & 0.4460 \\
0.0000 & 0.0000 & 0.0000
\end{bmatrix}
$$

To simplify the model, the four different bond lengths and valence angles were averaged over the optimum geometry of the dimer molecule. This gives $<l^2>$ as 2.07 Å^2 and the valence angle as 114°.

2.3.1.2. The Spatial Distribution of PHU Segments

The distribution of the normalized end-to-end distance, $W(r)$, is defined as the probability that the end-to-end distance is located between r and $r+dr$. Here, one chain end is placed at the origin of the coordinate system, therefore the probability that the end-to-end vector will be within a spherical shell of thickness dr is $W(r)4\pi r^2 dr$. Due to the spherical symmetry, the end-to-end vector, r, can be replaced with the end-to-end distance r. The end-to-end vector of the sufficiently long PHU chain in the unperturbed state can thus be shown to be Gaussian:

$$W(r) = \left[\frac{A}{2\pi\sigma^2}\right]^{\frac{3}{2}} \exp\left[-\frac{1}{2}\frac{(r-<r>)^2}{\sigma^2}\right]$$

(2.2)

Here, σ is the standard deviation of the end-to-end distance and $<r>$ is the ensemble average of the end-to-end distance, and A is the normalization constant satisfying the condition:

$$\int_0^\infty W(r)4\pi r^2 dr = 1$$

(2.3)

Here and elsewhere throughout the chapter, this distribution function will be denoted as "Gaussian distribution with a non-zero mean". A more specific form of the Gaussian distribution is the Gaussian chain for freely rotating chains. This is denoted as "Gaussian with zero mean" and defined as[2, 15]:

$$W(r) = \left[\frac{3}{2\pi <r^2>}\right]^{\frac{3}{2}} \exp\left[-\frac{3}{2}\frac{r^2}{<r^2>}\right]$$

(2.4)

The distribution generated by the RIS method shows the maximum at r/r_{max} ratio of 0.4, which is 0.25 for the ideal Gaussian chain with zero mean as shown in Figure 2.5. Here, the solid line represents the distribution generated by the RIS method, the dashed line is the fit to a Gaussian distribution with non-zero mean given in eq.2.2, and the dotted line is the fit of Gaussian with zero mean given in eq.2.4. Therefore, the spatial distribution of the PHU chain behaves like a Gaussian chain with non-zero mean. The larger end-to-

end distance is due to the long side chains and the partial double bond nature of the ester bond that leads to rotational hindrance.
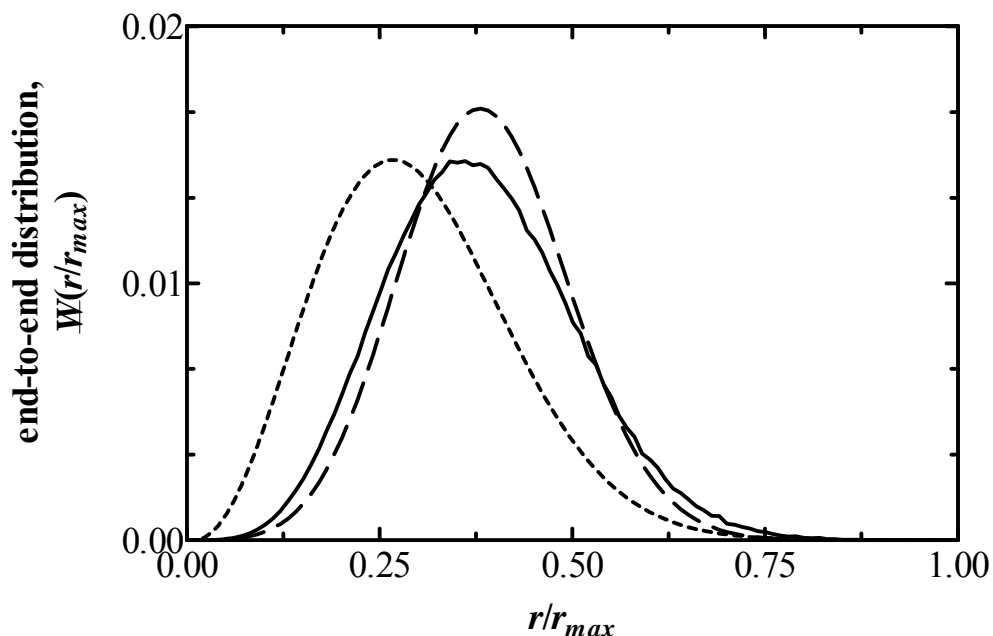
Figure 2.5. Distribution of normalized end-to-end distance of 150 repeat unit PHU chain generated by the RIS method (——), fitted to a Gaussian distribution with both non-zero (----) and zero mean (⋯⋯), where "mean" refers to $<r>$ in eqs. 2.2 and 2.4. Due to the large side chains, PHU shows persistence to higher dimensions with a non-zero mean.

2.3.1.3. Chain Dimensions

To monitor chain dimensions of the PHU molecule in the theta state, the characteristic ratio of the chains for an infinitely long chain, defined by $C_\infty = \lim_{n \to \infty} <r^2>_0/nl^2$, is calculated. Here, $<r^2>_0$ is the ensemble average of the square of the end-to-end separation in the unperturbed state, n is the number of bonds and l^2 is the square of the bond length, l. If the correlation between any of the neighboring bonds is zero, the chain behaviour is described by the freely jointed chain in which the root mean square end-to-end distance for a chain with n bonds is $<r^2>_0 = nl^2$

In the case of PHU, the conformation of the ith bond is strongly determined by the neighboring bonds, say $i+j$th bond. As j increases the correlation between the ith and $i+j$th bond vanishes. Thus, it can be represented by an equivalent freely-jointed chain.

For that purpose, a sequence of bonds is taken as the statistical element of the chain subject to the conditions that its root mean square end-to-end distance and the fully extended length r_{max} satisfy the conditions,

$$<r^2>_o = n' l'^{\,2} \tag{2.5}$$

and

$$r_{max} = n' l' \tag{2.6}$$

where, l' is Kuhn length and n' is the Kuhn segment. The persistence of an unperturbed chain is measured by the persistence length, l_p, where $l_p = l'/2$. In Figure 2.6, the characteristic ratio, $C_n(N)$, is presented as a function of the number of repeat units, N, with $N = 4n$.
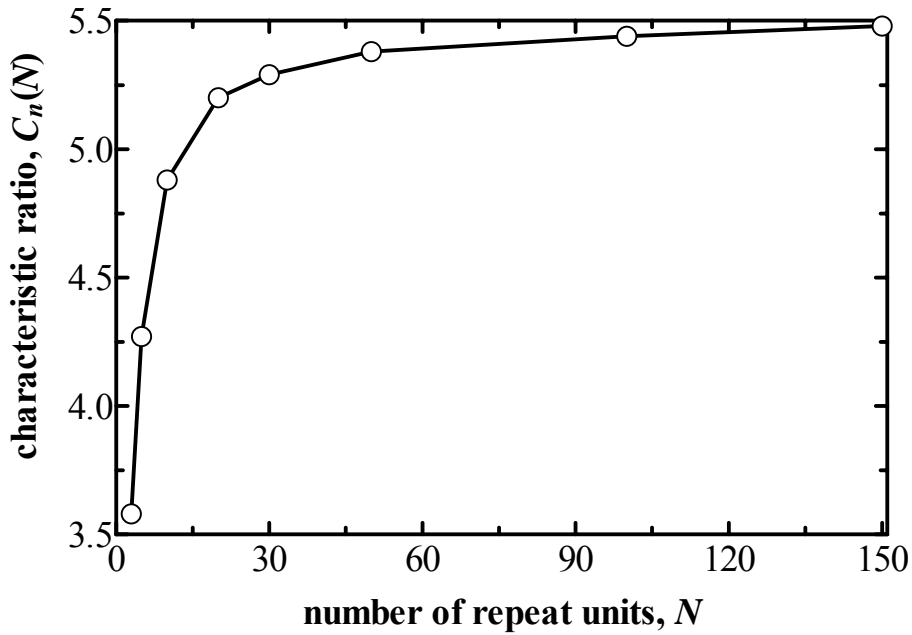
Figure 2.6. Characteristic ratio, $<r^2>/nl^2$, of the PHU chain of various sizes, calculated by the RIS model at 300 K. A line is drawn through the points to guide the eye. Only the short–range interactions are considered for chain growth to predict the unperturbed dimensions of the PHU chain. The value converges to the infinitely long chain as the chain size increases. The 30 repeat unit polymer, for which C_n is 95 % of C_∞ and is computationally manageable in size, is taken as the representative chain in all the subsequent calculations.

The open circles represent results of calculations, and the curve through the points is drawn to guide the eye. The C_n values reach to 5.3 for $n = 120$, which is 95 % of the asymptotic value for the PHU chain. For the range between 250 K - 400 K the temperature coefficient, on the other hand, is 1.3×10^{-3}. The characteristic ratio for PHB in theta solvent is ca. 7.5 and temperature coefficient is ca -1.4×10^{-3}[13]. The chain dimensions, r_{max}, $<r>$ and $<r^2>$, for the 100 repeat unit chain are 218 Å, 63.4 Å and 4512 Å^2, respectively. These values lead to the Kuhn length of 20.7 Å with 10.5 Kuhn segments for the PHU chain.

2.3.2. MD Simulations Results

2.3.2.1 Conformational Characteristics of a Single PHU Chain in Vacuum

To understand the conformational features of the PHU molecule, a dimer and a PHU chain with 30 repeat units were analyzed using MD simulations. The geometry of the dimer molecule, capped with H atoms at both ends, was optimized by carrying out a stringent minimization for each of the minima at the energy surface of the rotatable bond pairs discussed above. Detailed analysis of conformational characteristics show similarities with the theoretical studies performed for PHB. Marchessault and coworkers proposed the backbone dihedrals of the isotactic PHB as ttg^+g^+, whose repetition leads to helices. They report a 3.0 Å helical rise per repeat unit[9]. In our calculations for isotactic PHU, the rotational angles of the dimer, (ω, φ, ϕ, χ), are 3.5°, 107.7°, 7.2°, 93.2° respectively, and conform to the tg^+tg^+ state. We calculate the end-to-end distance of a repeat unit as 4.4 Å, and the helical rise per repeat unit as 3.9 Å. The more extended conformation of the backbone of PHU compared to PHB is attributed to the repulsive forces between adjacent bulky side-chains. Our calculations also predict stretched out side chains in the anti configuration with an end-to-end distance of 7.6 Å.

By using these parameters, we generated the initial configuration of the PHU chain. The convergence of the characteristic ratio in the MC study let us utilize 30 repeat units of PHU chain as a model throughout the MD simulations. This chain size is a good representative of the dimensions of an infinitely long chain, and is small enough to feasibly execute the simulations. After energy minimization, the optimum geometry of the PHU chain results in rodlike helices with geometric parameters in the vicinity of

the optimum dimer structure. At this local minimum C_∞ and Radius of Gyration of the backbone (R_g), which is defined as:

$$R_g = \left\{ \frac{1}{n} \sum (r_i - r_{CM})^2 \right\}^{\frac{1}{2}}$$ (2.7)

where, n is the number of backbone atoms, r_i is the distance of ith atom from the origin and r_{CM} is the center of mass of the polymer chain, is 44 and 34 Å respectively.

MD simulations of the single chain in vacuum at different temperatures indicate a sharp transition from helical rodlike to a randomly coiled globular structure. Figure 2.7 shows the evolution of R_g at temperatures 250, 300, 350 and 400 K in vacuum. This sharp transition is similar to the one observed in the ORD experiments when solvent quality decreases[11]. Independent of temperature, this transition occurs at around 50 ps. The calculated C_∞ values for the four simulations at 250 - 400 K lie in the ranges 0.3 - 1.6.

2.3.2.2. Conformational Characteristics of PHU Chain in The Bulk and Chloroform Solution

MD simulations have been successful in calculating the unperturbed dimensions and C_∞ value of the polyethylene terephthalate (PET) chains from the bulk state simulations[22]. Along similar lines, we analyzed the conformational features of PHU molecules in the unperturbed state with five chains, each having 30 repeat units. Periodic boundary conditions were applied in all directions so that the behavior of a sufficiently large system can be obtained. As shown in Figure 2.7, R_g converges to the value of 23 Å after 500 ps of equilibration with very small fluctuations around the equilibrium value. For PHB in the amorphous state, the C_∞ and l_p values were calculated as 18 and 19 Å respectively. The chain dimensions of the amorphous PHB, on the other hand, was observed as 39 and 31 Å from SANS experiments[14].
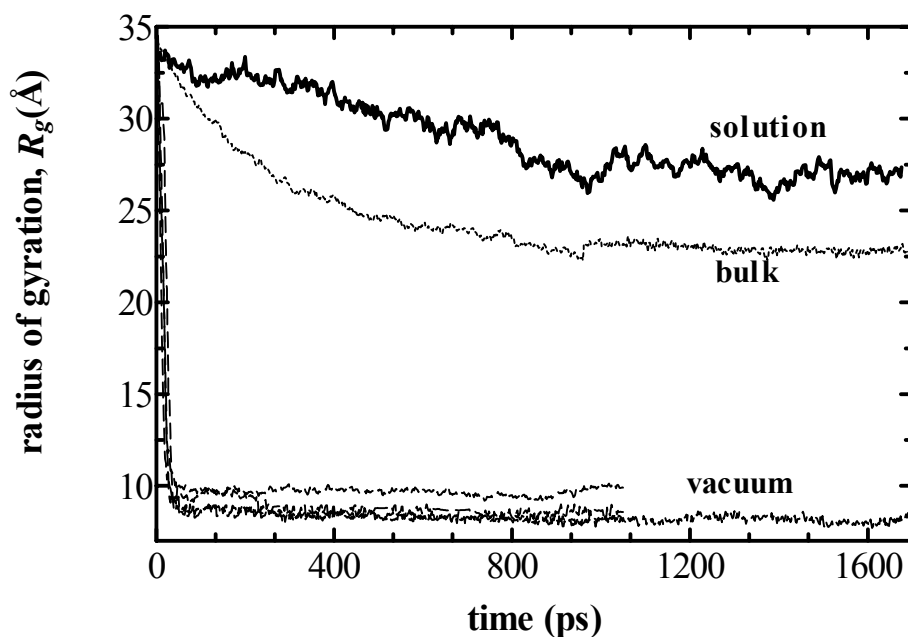
Figure 2.7. Radius of gyration of the backbone for the 30 repeat unit PHU chain as a function of time, calculated by MD simulations. Different runs are performed for PHU in chloroform solution at 300 K (1.7 ns), in the bulk state at 300 K (1.7 ns), and in vacuum at 250, 300, 350, 400 K (1.1 ns for the former three, 1.7 ns for the latter). The initial geometry is a rodlike helix whose rotational angles are in tg^+tg^+ state. In the vacuum, irrespective of temperature, helix to coil transition occurs in ca. 50 ps. In chloroform, fluctuations are higher, and the overall geometry is in the vicinity of the initial structure. The bulk environment is representative of PHU in the unperturbed state.

In chloroform solution, equilibration takes place in about 700 ps and fluctuations are higher than those found in both vacuum and amorphous simulations. The chain shows a strong preference for a rodlike conformation with a R_g of 27 Å. This size is ca. 20 % smaller than the R_g of the rodlike helical structure mentioned above and ca. 15 % larger than the bulk value. Finally, we observed C_∞ as 23 Å and l_p as 22 Å in solution.

2.3.2.3 Side Chains

The conformational characteristics of the seven repeat unit aliphatic hydrocarbon side chain are analyzed in terms of its end-to-end distance. For that purpose, distribution function of the end-to-end distance of each side chain in the 30 repeat unit PHU is analyzed for each MD simulation. The population shows a non-Gaussian behavior that is skewed towards larger chain lengths (data not shown). The skew is mainly due to the

two double bonds that restrict rotations and bias extension. The optimum geometry of the dimer structure obtained by energy minimization, reported in the "analysis of the single chain" subsection, has a 7.6 Å end-to-end distance, which is an extended structure for the side chain (the fully extended chain at its equilibrium bond lengths and angles would be ca. 7.7 Å). Independent of temperature, environment, and the backbone conformation, we always observe extended side-chains with end-to-end separation changing from 6.5 - 8.5 Å in all the MD simulations.

2.3.3 Comparison of RIS Model and MD Simulations

The results summarized above indicate that chain dimensions show differences depending on the environment. In vacuum, attractive interactions are overemphasized, thus resulting in small chain dimensions compared with the bulk and solution environments. The temperature, on the other hand, has no significant influence on chain dimensions in vacuum. The dimensions predicted by MD simulations in the amorphous state and in chloroform solution (a good solvent for PHU) are larger than those obtained from MC simulations.

Ideally, the chain behavior in the bulk state is representative of the unperturbed state. Thus, results from bulk simulations may be taken to correspond to chain behavior in theta solvent. On the other hand, RIS calculations for which only the short-range interactions are taken into account should also represent the unperturbed state in principle. The discrepancy between the two approaches (characteristic ratio is 5.3 and 18 from the RIS model and MD in bulk, respectively) is attributed to the incomplete treatment of the side chains in the RIS model: PHU chains have bulky side chains, but during MC chain generation the excluded volume interactions among neighboring side-chains are not considered, resulting in the estimation of lower chain dimensions in the RIS model.

2.3.4. Distribution of Dihedral Angles

Among the three local geometric variables, the bond length, the valence angle and the dihedral angle, only the dihedral angle has significant effects on the overall conformation of a chain. We find that the dihedral angle shows differences as the

temperature and environment change in the simulations. Therefore, a detailed analysis of dihedral angles leads to an understanding of the structural changes, the dynamics, and the flexibility of the chains. The role of temperature and environment on the population of the rotational angles is investigated from the ensembles generated from the MD simulations. In all simulations, the partial double bonded ester bond is observed to be in *trans* form with fluctuations around $\pm 60°$. This behavior is independent of the temperature and the environment. The populations of other dihedrals (φ, ϕ, χ) as a function of dihedral angle in degrees are summarized in the Figures 2.8-2.10; we will elaborate on the details of these figures below. The effect of the environment (vacuum, bulk, or solvated) at the constant temperature of 300 K is shown in the figures, whereas the temperature effect is displayed in the insets. Note that, since the behavior of the chain at 350 K and 400 K is nearly the same for all four types of dihedral angles, only the results from the 400 K simulations are shown in these figures.

The rotation around the O-C bond, represented by the φ angle, varies as the conditions are changed. The RIS model estimates two predominant conformers, *t* and g^+, with populations 0.27 and 0.73, respectively. Similarly, all the MD simulations reflect the preference of the φ angle towards the *t* and g^+ states, as shown in Figure 2.8.
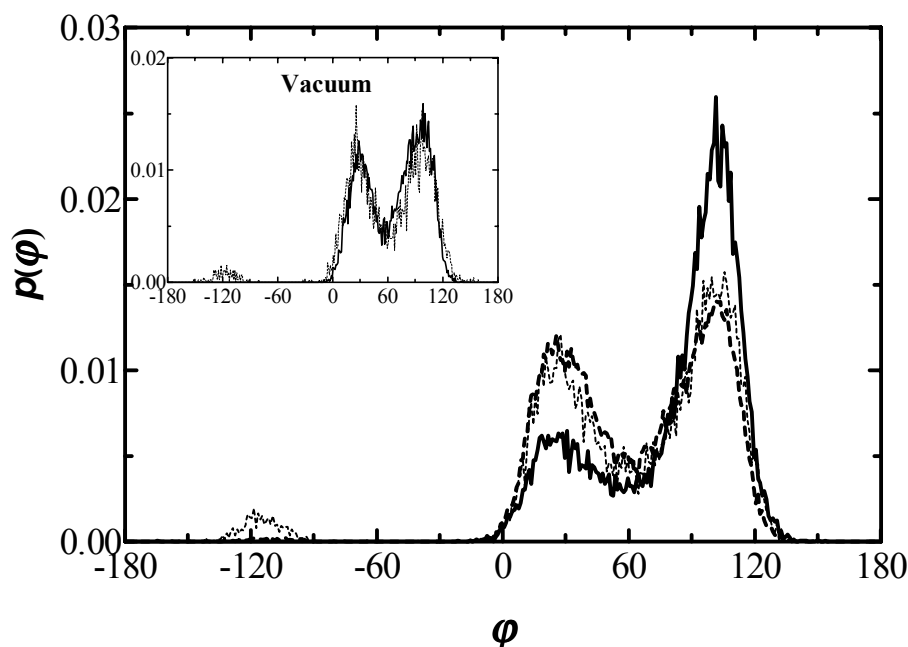
Figure 2.8. φ angle distribution calculated from MD simulations. In vacuum at 300 K (- ---), *t* and g^+ states have equal probabilities, while in chloroform solution at 300 K (——) g^+ is favored. The bulk state at 300 K (·······) shows the same behavior as the chain in vacuum at 400 K. The inset shows the vacuum behavior of PHU at 250 K (——) and 400 K (·······); a minor population arises at the g^- state at higher temperatures.

As the temperature is changed from 250 K to 400 K, the g^+ population is slightly reduced from 0.61 to 0.49; also, a slightly populated g^- state emerges at the higher temperatures (see inset of Figure 2.8). The role of the environment on the statistics of φ is more significant. The behavior of the bulk phase, studied at 300 K, is similar to the behavior of chains in vacuum at 400 K. Finally, in chloroform, where the g^- state is not populated, the dihedral distribution of φ shows a distinct preference for the g^+ state with a t:g^+ probability ratio of 0.25:0.75, very similar to the RIS model result.

We observe two dominant states for the ϕ angle in the MD simulations. The states t and g^- are the two minima that emerge in the probability matrix of the RIS calculations. These two minima are also significantly populated in the MD simulations (Figure 2.9). Here, the $g^- \leftrightarrow t$ transition occurs easily at every temperature and in every environment. In vacuum, a slight preference for the g^- state is observed. In addition, at
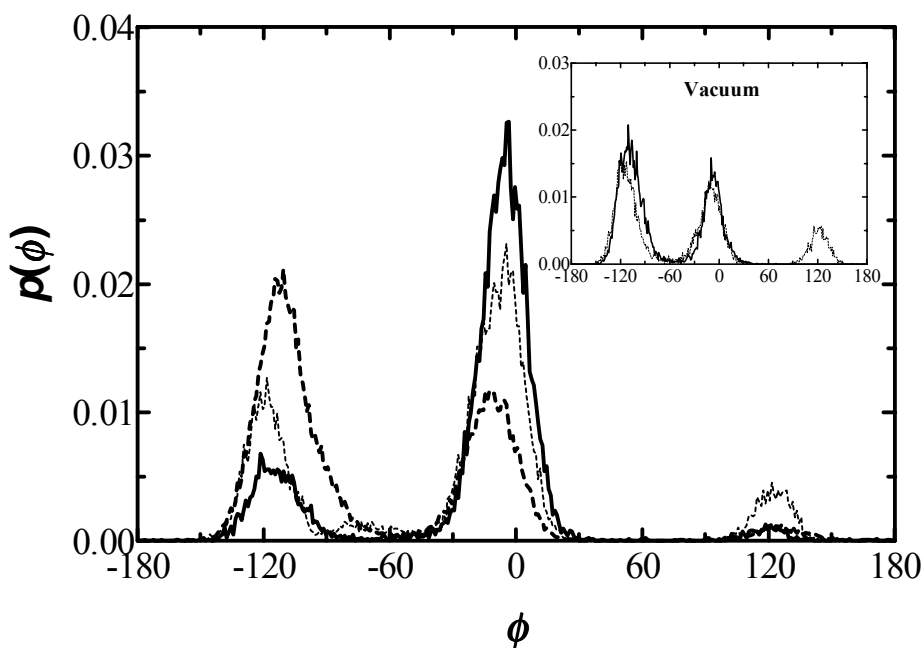
Figure 2.9. ϕ angle distribution calculated from MD simulations. In vacuum at 300 K (-
---), g^- and t states are favored, while in chloroform solution (——) and the bulk state at 300 K (·······) the t state is predominant. The inset shows the vacuum behavior of PHU at 250 K (——) and 400 K (·······); at higher temperatures three states are populated while at low temperatures g^- and t are favored.

250K, the energy barrier to g^+ cannot be surmounted. As the temperature is increased, probabilities of the two states become closer to each other and the population of g^+ increases (inset of Figure 2.9). The environment again has a more pronounced effect on

the population of the φ angle. In the bulk and solution the *t* state is overpopulated, in contrast to the vacuum case. The probability of *g⁻*:*t* in vacuum is 0.76:0.22 while for the bulk and solution it is 0.29:0.63 and 0.17:0.81, respectively. Interestingly, in the RIS calculations, this ratio is 0.59:0.40, i.e. there is a slight preference to the *g⁻* state.

The distribution of the χ angle, displayed in Figure 2.10, has two maxima at *g⁻* and *g⁺* under all conditions. Due to its high energy, as corroborated by the RIS model, the *t* state is not populated. At 250 K, *g⁺*:*g⁻* has a ratio of 0.78:0.09, while as the temperature is increased to 400 K, this ratio changes to 0.45:0.46. Note that approximately 10 % of the conformations lie in the range −60° < χ < 60° (inset of Figure 2.10). In addition, an increase in temperature results in a broadening of the
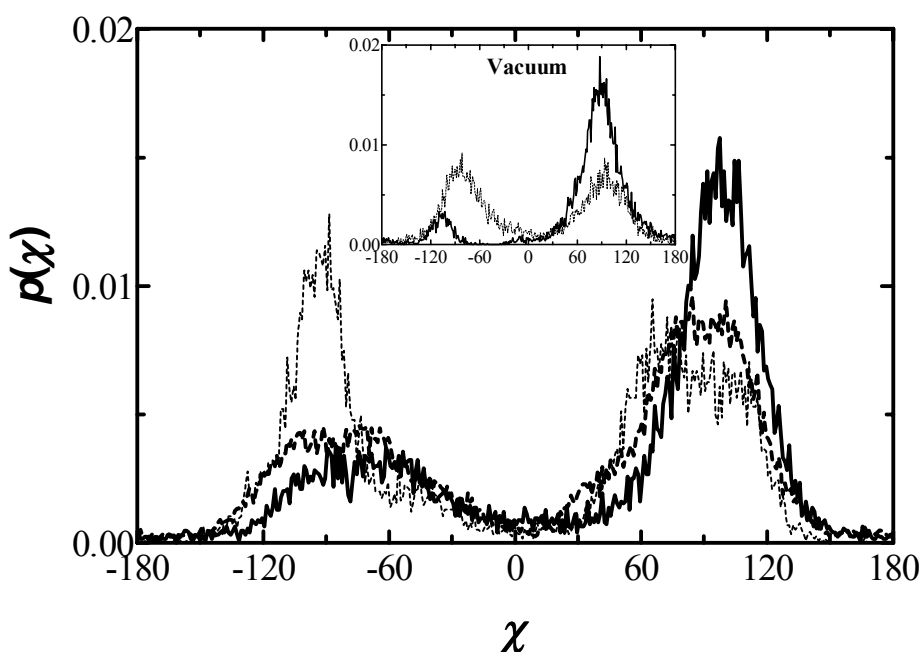
Figure 2.10. χ angle distribution calculated from MD simulations. In vacuum at 300 K (----) and in chloroform solution at 300 K (——), *g⁺* and *g⁻* are favored with a preference towards the former. The bulk state at 300 K (······) shows the same behavior as the chain in vacuum at 400 K; here *g⁺* and *g⁻* states have equal probabilities. The inset shows the vacuum behavior of PHU at 250 K (——) and 400 K (······); the preference of the *g⁺* state at lower temperatures shifts towards an equal distribution of *g⁻* and *g⁺* as the temperature is increased.

available states. In comparing the distribution of χ in different environments, we observe that the distribution of χ in the solvent favors the *g⁺* state (Figure 2.10) with a *g⁻*:*g⁺* ratio of 0.18:0.73. In contrast, the amorphous state behaves like the chain in

vacuum at 400 K and we observe the g^- state confined to a narrow range with a $g^-:g^+$ ratio 0.46:0.50. This ratio is 0.32:0.68 in the RIS calculations.

2.3.5 Helix Formation

The detailed study of rotational angles, outlined above, indicates that ω has access to the t state only, while each of the other three angles, φ, ϕ, χ, may be found in two probable states. This results in eight different combinations of rotational angles, (ω, φ, ϕ, χ), for the backbone of the PHU molecule: $tttg^-$, $tttg^+$, ttg^-g^-, ttg^-g^+, tg^+tg^-, tg^+tg^+, $tg^+g^-g^-$, $tg^+g^-g^+$. If any of these combinations repeats persistently along the chain, a helical structure will emerge; otherwise, a randomly coiling structure is expected. To comprehend the helicity of the chain, we recorded the number of times these combinations repeat along the backbone. From the eight conformations, only the combination tg^+tg^+ occurs more than 1% during the simulation. We define helix length as the consecutive number of repetitions of the tg^+tg^+ state, given as percent of the total chain length. We also define helix persistence as the percent of simulation time during which a certain helix length is observed in the trajectory. To remove end effects, two repeat units from each end are discarded. Results for different temperatures and media
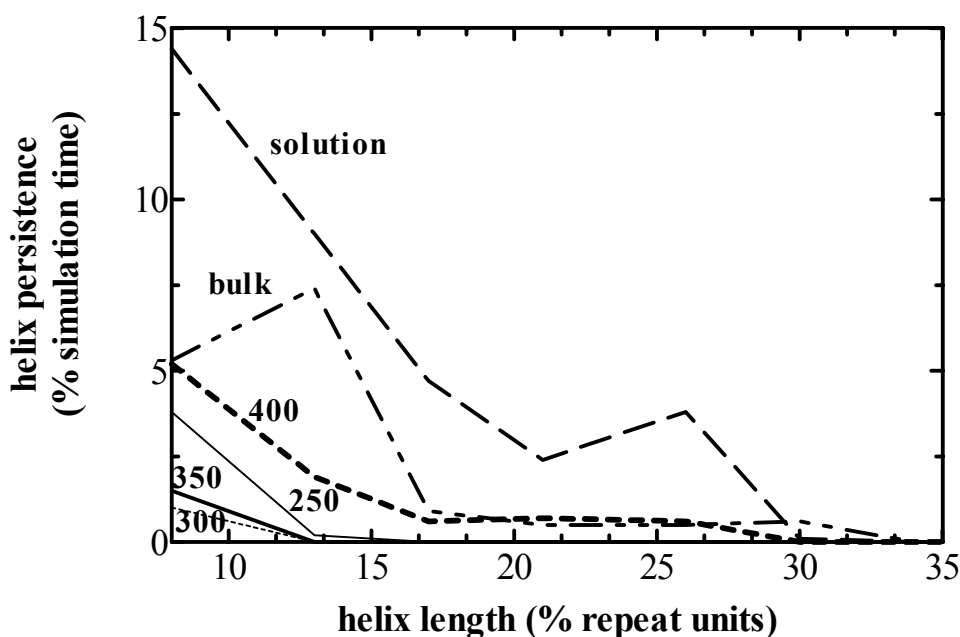
Figure 2.11. Helix persistence as a function of helix length calculated from MD simulations for PHU chains of 30 repeat units at different temperatures and in different environments. In vacuum, irrespective of temperature, helix formation is not significant.

In chloroform, which is representative of a good solvent for PHU, the chain has considerable helix persistence. There is some helix formation in the bulk state, but it is not as pronounced as for PHU in good solvent.

are summarized in Figure 2.11. Here, helix persistence as a function of helix length is shown for PHU chains of 30 repeat units. The labels on the figure represent the environment or the temperature of the simulations. The labels, solution and bulk, represent the chain behavior in chloroform solution and the amorphous state, respectively, at 300 K. The other labels (250 K, 300 K, 350K and 400K) represent the behavior of chain in vacuum at the specified temperature. Curves are drawn through the points to guide the eye. Here, we see an insignificant amount of helix formation at all temperatures in vacuum. In the bulk phase and in solution, longer stretches of helical segments are observed. In particular, chains in the solution environment have considerable helix persistence.

3. CONFORMATIONAL AND DYNAMIC PROPERTIES OF NOVEL SURFACTANT MOLECULES DESIGNED FOR CO$_2$ APPLICATIONS AT SUPERCRITICAL CONDITIONS

3.1. Overview

Supercritical fluids (SCFs) offer a series of technical advantages in extraction and separation; they can also be used as a reaction medium. Carbon dioxide (CO$_2$), because of its low cost, low toxicity, and readily accessible critical point (T_c = 31° C, P_c = 73.8 bar), is the ideal solvent for the SCF applications. In addition, CO$_2$ is easily recyclable and can be removed from the reaction systems through simple depressurization at ambient temperatures, allowing for low-energy, low-cost processing protocols[23]. However, because of its very low dielectric constant, and polarizability per volume, CO$_2$ is a poor solvent for most non-volatile lipophilic and hydrophilic solutes. Only the molecules that have low cohesive energy densities such as fluorocarbons, fluoroethers, siloxanes[24] polycarbonates[25] are soluble in CO$_2$. Researchers have turned to concentrate on developing polymeric and small molecule amphiphiles. These amphiphiles generally contain a CO$_2$ - philic unit that can disperse in bulk solvent and a CO$_2$ - phobic unit that tends to sequester away from CO$_2$ and can associate with solids[26, 27]. It is possible to disperse either liphophilic or hydrophilic phases into CO$_2$, in terms of microemulsions, emulsions and latexes, by appropriate surfactants. The design and characterisation of surfactants that enhance the solubilization of liphophilic and hydrophilic phases in CO$_2$ is therefore crucial for its extensive application[28]. Most of the industrially available surfactants are incapable of forming stable micelles in CO$_2$ because of their negligible solubility[29]. For this reason, significant research effort has been directed to prepare surfactants that have CO$_2$ - philic and hydrophilic or hydrophobic segments[28].

Molecular simulation techniques have been applied for understanding the structure, rheology and dynamics of aqueous surfactant systems for a long time. Molecular modelling of small amphiphiles contributed in understanding (i) the T_1 and T_2 relaxation times in NMR[30, 31], (ii) micelle size and shape in small angle neutron scattering (SANS)[31-33] and (iii) dynamics of micelle formation in diffusion experiments[34]. Compared to the huge experimental effort devoted to the study of surfactants in SCCO$_2$ [35], theoretical studies are far from being sufficient[36]. The self-assembly behaviour and micelle formation in SCCO$_2$ are based on intermolecular interactions between solute and solvent molecules described as an entropy driven process[37, 38]. Most of the studies that investigate the micelle formation[39] and self-assembly of surfactants in supercritical solvent-surfactant systems utilize coarse-grained Monte Carlo (MC) simulations due to the large system size and demanding time needed to observe self-organisation. There are some attempts to use large-scale coarse-grained molecular dynamics (MD) simulations to understand the process of micellization in SCCO$_2$[40-42], but in these studies molecular specificity is ignored. As a result, some aspects of real systems such as concentration dependence of self-assembly cannot be reproduced well[43]. In their paper series, Salaniwal and co-workers[44-46] studied intermolecular interactions and dynamics of micelle formation by multichain simulation of the dichain surfactant, $(C_7F_{15})(C_7H_{15})CHSO_4^-Na^+$ – water system in SCCO$_2$. Results of their studies are consistent with the SANS experiments performed on the same system[47]. Recently, single chain MD simulations were performed by Baysal et al. to study the conformational properties of single chain diblocks of poly1,1-dihydroperfluoro-octyl acrylate and polyvinyl acetate in SCCO$_2$[48]. The pressure dependence of solubility, reported in laser light scattering and synchotron small angle x-ray scattering (SAXS) experiments[49-51], is successfully verified and the role of intra-chain interactions on the micellization process is emphasized for the first time.

In this chapter, we designed a precursor to prepare oligomers, which contains fluorinated segments by utilizing a macroperoxide initiator. The details of reaction steps and reaction schema are given in Figure 3.1. Before going further into preparation of different fluorinated oligomers, it is desirable to determine their phase-solubility behaviour in liquid and supercritical state. Therefore, we utilize single chain MD simulations on 10 different types of co-oligomer chains in explicit CO$_2$. The spatial configuration of each segment and their detailed structural analysis due to solvation are
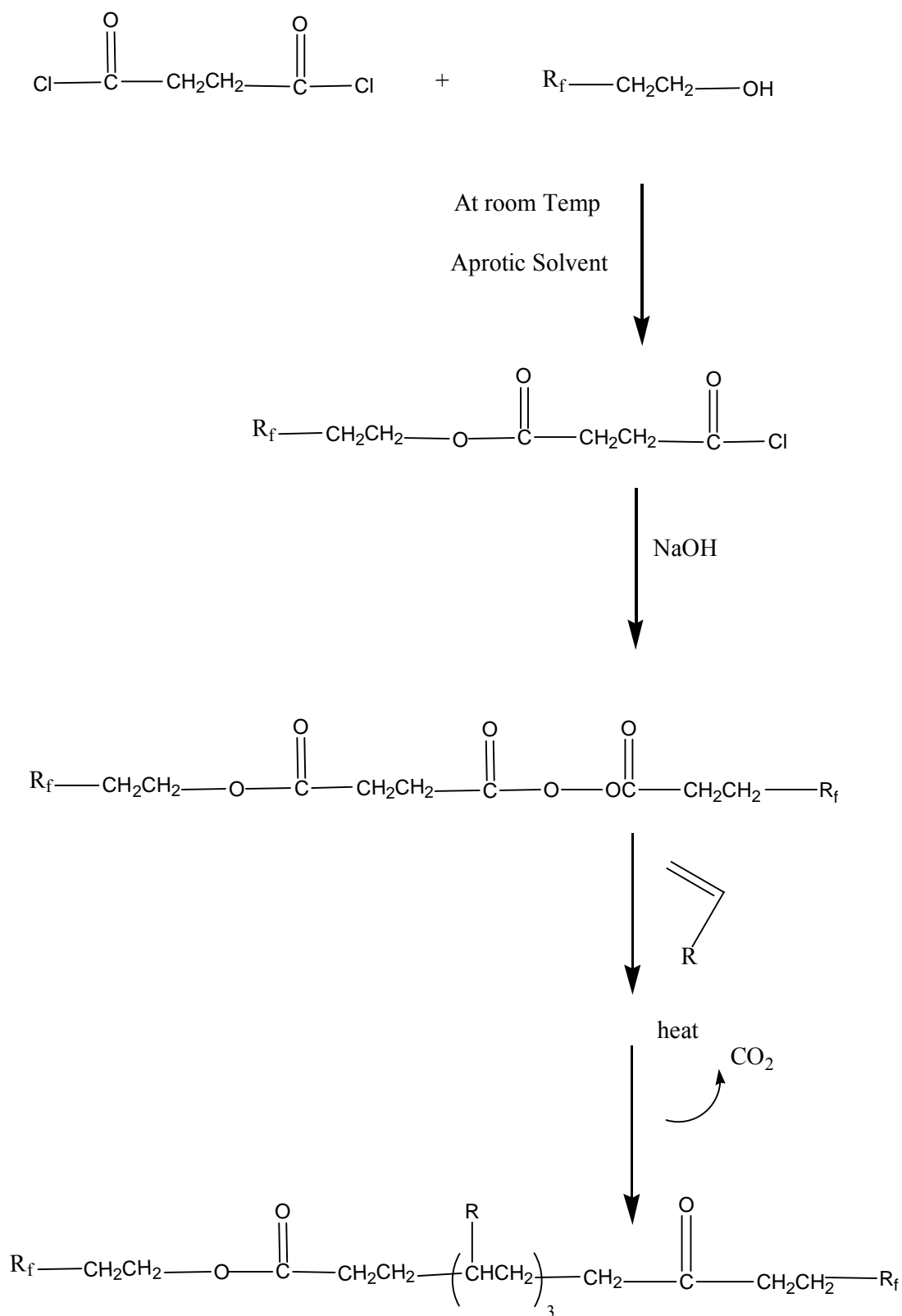
Figure 3.1. Reaction schema of the novel surfactant oligomers by using macroazoinitiator. Here –R represents the 10 different monomers utilized in calculations.

investigated. The overall dimensions and the dynamics of the CO_2 - philic and CO_2 - phobic parts are reported. The effect and behaviour of different functional groups in the $SCCO_2$ environment is discussed to provide some detailed insight into the solvation mechanism.

3.2. Molecular Model and Computational Methods

3.2.1. Molecular Models

The molecular models that are used in this study are oligomers, which can be prepared by commercially available monomers. We utilize ABCBA type oligomers (Figure 3.2) where the A blocks are CO_2 - philic blocks of C_8F_{17} (hepta decafluorooctyl) whereas the B and C blocks are the CO_2 - phobic ethyl propionate and ethylene co-oligomers with the respective generic formulas $(CH_2)_2(OCO(CH_2)_2)$ and $(CH_2CHR)_3$.
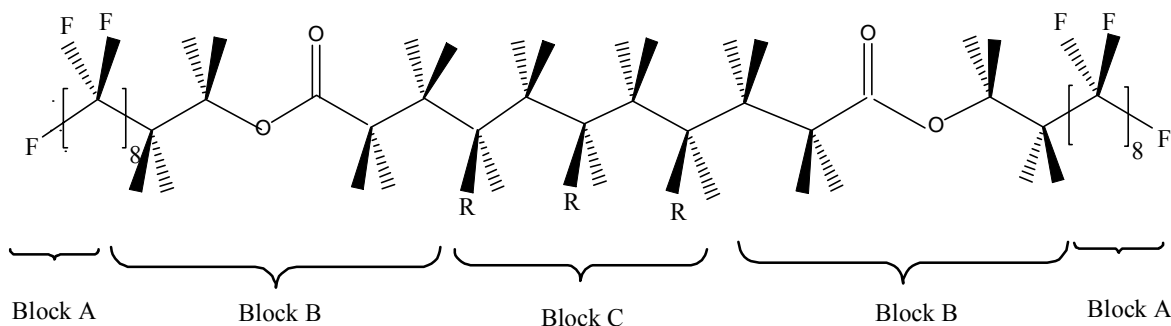
Figure 3.2. Molecular structures of ABCBA type model surfactant oligomer.

In the C block, 10 different commercially available monomer types (-R) listed in Figure 3.3 are studied. These monomers have different chemical properties; group 1, 2, 3, 4 and 6 show hydrophobic and non-ionic character while group 5, 7, 8, 9, 10, are ionic and hydrophilic. The size, polarity and degree of hydrophobicity/hydrophilicity, also vary in the same group, thus different properties and application areas are expected for each system.
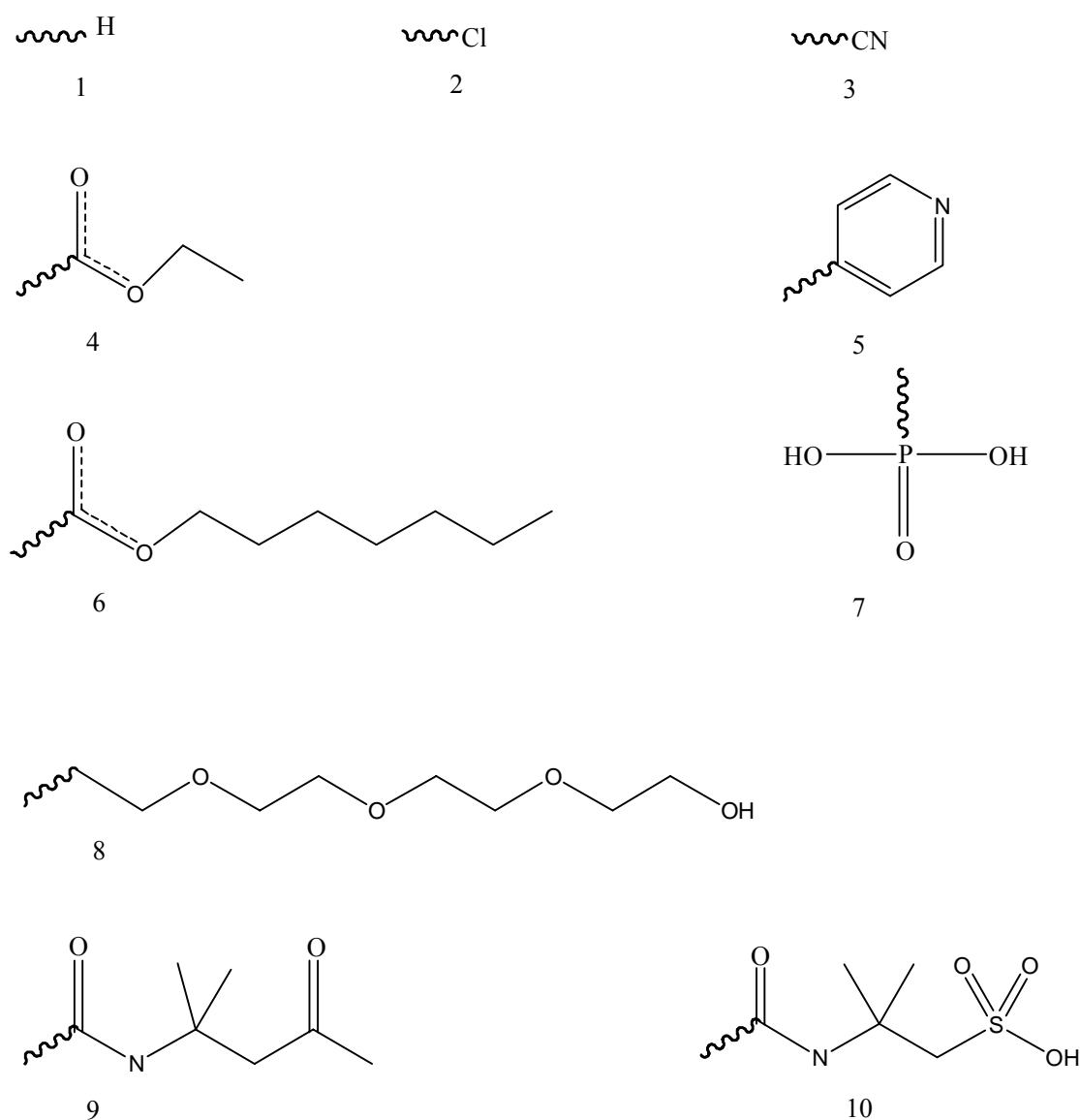
Figure 3.3. Molecular schemes of monomer types utilized in the CO_2 – phobic segment

3.2.2. MD Simulations Method

All MD simulations are carried out with the Molecular Simulation Inc. Insight II 4.0.0P software package. Periodic boundary conditions with a cut-off radius of 9.5 Å for all nonbonded interactions are employed in the canonical ensemble (NVT). For pressure and energy calculations, van der Waals tail corrections are made[20]. Initial velocities are assigned from a Maxwell-Boltzmann distribution in such a way that the total momentum in all directions sum up to zero. To choose a suitable forcefield that will best represent the system under the given conditions, preliminary MD simulations are performed on a pure CO_2 system of 1000 molecules at a density of 0.76 g/cm^3 using the

Consistent Valence Forcefield (CVFF)[52], Consistent Forcefield 91 (CFF91) [53], and Polymer Consistent Force Field (PCFF)[16, 17] and various temperature control protocols. From those, the PCFF forcefield with the Nosé temperature control method[21] is used in the rest of the study, as these lead to the best estimate of the experimentally observed pressure at this temperature and density for pure CO_2 ($T = 300$ K, $P = 80$ bar). This forcefield and temperature control method combination also leads to the smallest fluctuations in pressure.

All the geometries of the oligomers are initially optimized in vacuum by Conjugate Gradients method up to a final convergence of 0.05 kcal/mol/Å. In all calculations, each oligomer, with size ranging from 102 to 188 atoms, is immersed in a cubic box of 1000 CO_2 molecules. Thermodynamic conditions of simulations are adjusted in 0.76 g/cm^3 and 300 K so that the systems mimic the experimental pressure and temperature at the near supercritical point. After generation and minimization of all the CO_2 oligomer – systems with Conjugate Gradients method up to a final convergence of the potential derivative of 0.1 kcal/mol/Å, a 0.9 ns of MD simulation is performed for each system. The time step is taken as 1 fs and the positions of the atoms are recorded at every 2 ps for detailed analysis. First 100 ps of the run is discarded to remove bad contacts and the effect of initial configurations on the systems. The remaining 0.8 ns of simulation time is found to be adequate to monitor the local chain dimensions and dynamics, since the time correlations of local segments are on the order of 100 ps.

3.2.3. Calculation of the Principal Axes

To investigate the overall shapes of the equilibrium structures, the three principal axes of the oligomer backbone were calculated and the projections of the equilibrium structures along these axes were considered. Here, our aim is to find the basis vectors of matrix $\mathbf{A}_{3xn}(j)$, where n is the number of atoms in the system and each column of $\mathbf{A}^T_{nx3}(j)$ constitute the $\mathbf{x}$, $\mathbf{y}$, and $\mathbf{z}$ components of configuration j. Accordingly, a basis set constructed by singular value decomposition is utilized[54]. Thus, $\mathbf{A}_{3xn}(j)$ is written as,

$$\mathbf{A}_{3xn}(j) = \mathbf{U}_{3x3}\mathbf{W}_{3x3}\mathbf{V}_{3xn}^T \qquad (3.1)$$

Here the columns of the **U** matrix, denoted by $\mathbf{u}_i$, are the left singular vectors of **A**, whereas the columns of **V**, denoted by $\mathbf{v}_i$, are its right singular vectors. Note that $\mathbf{u}_i$ and $\mathbf{v}_i$ are orthogonal; i.e.,

$$\mathbf{U}^{\mathrm{T}}\mathbf{U} = \mathbf{U}\mathbf{U}^{\mathrm{T}} = \mathbf{E}_{3x3}; \qquad \mathbf{u}_i^{\mathrm{T}}\mathbf{u}_j = \boldsymbol{\delta}_{ij}$$
$$\mathbf{V}^{\mathrm{T}}\mathbf{V} = \mathbf{V}\mathbf{V}^{\mathrm{T}} = \mathbf{E}_{nxn}; \qquad \mathbf{v}_i^{\mathrm{T}}\mathbf{v}_j = \boldsymbol{\delta}_{ij}$$

(3.2)

where, $\mathbf{E}_{mxm}$ is the identity matrix of order m and δ_{ij} is the Kronecker delta. **W,** in eq 3.1, is a diagonal matrix with non-negative elements, $\mathbf{w}_i$, which are the singular values of **A**. The left singular vector associated with the largest singular value points out the most dominant direction, whereas the right singular vectors are the projections of **A** along the singular vectors. Thus, the orthogonal vectors defined by $\mathbf{u}_i$ give the three principal axes of the molecule, whereas the size of the associated elements of $\mathbf{w}_i$ provide the contribution, p_i, of each vector to the overall shape of the molecule by,

$$p_i = \frac{w_i}{\sum w_i}$$

(3.3)

where, for example, a small p_i means the orientation of the molecule along the related principal vector is negligible. Thus, the contribution fraction of a given conformation along the three principal axes is evaluated from the size of the eigenvalues belonging to each principal axis. In this context, equal contributions along the three axes represent a spherical shape, a large contribution from one axis and a minor contribution from the other two represent a rodlike shape and two significant contributions from two axes together with one minor contribution from the third represents a planar bidirectional shape.

3.2.4. Radial Distribution Functions

The structure of the solvent molecules around the oligomer may be investigated by utilizing radial distribution functions (RDF), $g_{ab}(r)$:

$$g_{ab}(r) = \rho_{ab}(r) / <\rho_a> \tag{3.4}$$

where $\rho_{ab}(r)$ is the number density of finding particle a around particle b at a distance of $r \pm dr$ and $<\rho_a>$ is the average number density of a. Thus, $g_{ab}(r)$ is a measure of the extent to which the solvent density around the oligomer deviates from the bulk density $[g_{ab}(r) = 1$ as $r \rightarrow \infty]$. RDF is of central importance in the thermodynamics of oligomer solutions, because it contains information on the global character of intermolecular interactions and gives detailed information on the interaction potential as a function of the separation between the two centers of mass. RDFs can be extracted from x-ray and neutron diffraction experiments[55] and as well as MD simulations[3, 4, 20]. Since MD provides positions of atoms as a function of time, $g_{ab}(r)$ can be directly calculated by the formula:

$$\rho g_{ab}(r) = \frac{2}{N}\left\langle \sum_i^N \sum_{j<i}^N \delta[r - r_{ab}] \right\rangle \tag{3.5}$$

Here N is the total number of atoms, ρ is the number density of the system, r_{ab} is the distance between centers of atoms a and b and angular brackets represents a time average. In practice, the RDF is computed by compiling a histogram of all pair seperations falling in predetermined distance ranges. In this study, we take the C atom of the CO_2 molecules as a and selected atoms along the backbone of the oligomers as b.

3.2.5. Energetics of the Solubility

To form a stable oligomer – solvent system, the Helmholtz free energy of mixing, $\Delta F_{mix} = \Delta E_{mix} - T\Delta S_{mix}$, must be negative and at a minimum. ΔE_{mix} is the change in the internal energy of mixing, which depends on the solution density, and solvent–solvent, oligomer–solvent and oligomer–oligomer interaction energies. ΔS_{mix}, on the other hand, is the change in the entropy of mixing and depends both on the change in the chain conformation upon solvation, and the structure of the solvent around the oligomer. However, calculating the two terms accurately is a challenging task and is not the subject of this study. Here, we will focus on the energy change when the oligomer is immersed in the solvent to understand the specific interactions between the oligomers and CO_2. For that purpose, nonbonded energies, E_{nb}, are calculated for the system

33

including both oligomer and solvent. Assuming further that the interaction energies are additive, the contributions from oligomer–oligomer interactions, $E_{O/O}$, and solvent–solvent interactions, $E_{CO2/CO2}$, are subtracted from the total nonbonded energy to make an estimate of solvent–oligomer interactions:

$$E_{CO2/O} = E_{nb} - E_{CO2/CO2} - E_{O/O} \qquad (3.6)$$

Although this is a crude approximation to the strength of the interactions between the solvent and the oligomer, it will give a prediction of the energetics of the ongoing phenomena.

3.2.6. Dynamics of Chain

The dynamics of certain segments of the oligomers are analysed by the time decay of bond autocorrelations. For a given bond i along the backbone, the orientational autocorrelation function, OACF, is defined by

$$C_i(t) = <u_i(t_o) \cdot u_i(t_o+t)> \qquad (3.7)$$

Here $u_i(t_o)$ is the unit vector along the bond of interest at time t_o, and the brackets denote the time average over the ensemble. Thus, averages are taken over all snapshots with a time delay of t between them. $C_i(t)$ is related to the dielectric relaxation process[56, 57]. Nuclear magnetic resonance (NMR) measures the time correlation functions of magnetization, which is related to the reorientation of particular bonds in the polymer molecule; inelastic neutron scattering experiments measure the time correlation functions of the atom positions, infrared and Raman scattering spectroscopies measure the time correlation functions of the dipole moments and polarizabilities of the molecules. If the relaxation function may be characterized by a single phenomenon, it can be modelled with a simple exponential with a single rate constant. However, usually $C_i(t)$ will have contributions from different homogeneous processes with different relaxation times, and their collective effect on relaxation will be observed as heterogeneous dynamics[58, 59], represented by

$$C_i(t) = \sum_{i=1}^{n} \exp\left(\frac{-t}{\tau_i}\right) \qquad (3.8)$$

the above equation may be approximated by the stretched exponential, or the Kohlrausch-Williams-Watts (KWW) function[56, 60]

$$C_i(t) = \exp\left[(-t / \tau_i)^\beta\right] \qquad (3.9)$$

β ($0 \leq \beta \leq 1$) is a measure of the complexity of the processes contributing to the memory loss of the decaying vector. $\beta = 1$ for a system showing simple exponential decay, and decreases for more complex dynamics. τ_i is the characteristic time for the relaxation of bond i, reflecting the average relaxation time of the contributing processes.

3.3 Results and Discussion

3.3.1 Conformational Characteristics of the Oligomers

To investigate the local chain geometries in poor solvent, it is conventional to go to the vacuum extreme where the solvent effect does not exist. The conformational features in this extreme are important for understanding the role of the solvent on chain structure. For that purpose, we performed a molecular mechanics study on the structures of the surfactants in vacuum and analysed the equilibrium structures of the CO_2 - phobic and CO_2 - philic parts. The equilibrium geometry of the middle segment (BCB in Figure 3.2) varies with the size of the side chain. The oligomers with the short and linear side chains (see Figure 3.3), 1, 2, 3, 4 and 5, obtain a rodlike shape with the radius of gyration (R_g) of the backbone carbon of ~10 Å. The oligomers with longer and branched side chains 6, 8, 9 and 10 have larger size; thus, the larger nonbonded interaction contribution results in the shrinkage of the middle segment to a R_g of ~8 Å. In the case of 7, the side-chain size is relatively small, while R_g is ~8.5 Å due to the pronounced electrostatic interactions between phosphite ions on adjacent chains. Each fluorinated

block, on the other hand, attains a rodlike geometry with R_g of ~5 Å in every system and the character of the middle segment does not effect these blocks.

The surfactant chains show similarities when they are simulated in the CO_2 environment and R_g is taken as a measure of size. In the BCB segments, we observe ca. 30 % decrease in the R_g excluding types 7 and 8. Type 7 shrinks to a smaller R_g, which is ca. 50 % less than the vacuum value, while type 8 shows no significant change in the CO_2 environment. The CO_2 – philic fluorinated block acquires the same size and shape as in the vacuum environment with small fluctuations around the equilibrium value. The rodlike behaviour and small fluctuations indicate that the bulky fluorine atoms restrict the rotations and resulted with a stiff CO_2 – philic tail.

Due to the fluctuations in the systems, it is difficult to classify the shape of the molecules and its segments by monitoring the trajectories. As a measure of shape, we evaluate the time evolution of the contribution fraction of the principal axes and its average over 0.8 ns of dynamics run. The results are summarized in Table 3.1 for the oligomers studied. The fluorinated blocks in all the chains acquire a large contribution from one axis (82 %) and a minor contribution from the other two (12 and 6 %) that indicate a predominantly rodlike shape. Compared with the fluorinated blocks (A), the shape of the CO_2 – phobic segment (BCB block) is always ellipsoidal, with an average of 62, 28 and 10 % contribution to the three axis. Moreover, irrespective of the character of the side chains, molecules as a whole are also planar and ellipsoidal, that is, the two fluorinated blocks are like arms contained within the same plane as the BCB block. This behavior is quantified by the contribution fraction of the pricipal axes (60, 28, 12 %, see Table 3.1 for details).

We also monitored the flapping motion of the fluorinated arms for each of the oligomers. We define an *open structure* as one in which the distance between the two ends of the whole chain is larger than at least 1.2 times the distance between the two ends of the middle segment. Depending on the specific interactions, the chains alternate between open and closed structures in time. Among the structures, types 1, 2, 4 and 8 prefer the open forms more than 90 % of the time. The rest of the oligomers alternate between open and closed forms. Types 3, 9, and 10 have open and closed forms ca. 50 % of the simulation time, whereas 5, 6, and 7 have a preference towards the open form (70 % open vs. 30 % closed).

All of the conformational features outlined above point to the fact that the main factor controlling chain conformation is the backbone. Moreover, if we consider oligomer 1 as the control case due to its lack of the R-groups in the middle segment, the

Oligomer	CO_2 – phobic segment	Whole oligomer
1	0.70/0.21/0.09	0.68/0.23/0.09
2	0.63/0.26/0.11	0.61/0.27/0.12
3	0.55/0.33/0.12	0.56/0.29/0.15
4	0.68/0.22/0.12	0.66/0.24/0.10
5	0.69/0.22/0.10	0.62/0.25/0.15
6	0.59/0.30/0.11	0.56/0.30/0.14
7	0.51/0.35/0.15	0.54/0.31/0.15
8	0.60/0.29/0.12	0.63/0.26/0.11
9	0.65/0.26/0.09	0.59/0.31/0.10
10	0.57/0.33/0.10	0.54/0.29/0.17

Table 3.1. Contribution fraction of the three principal axes of the CO_2 – phobic block and the whole oligomer backbone. The contribution of the CO_2 – philic block is 0.82/0.12/0.06 for all cases with an uncertainty of 0.01. Results are averaged over 0.8 ns of MD runs.

stable overall structure expected from this backbone construction is a bidirectional ellipsoid with an open arrangement of the fluorinated blocks. Specific interactions caused by the special entities along the side chains have secondary importance, and they cause such changes as the mild shrinkage of the middle segments (eg. oligomer 7) or destabilization of the open form to cause large scale fluctuations of the two ends.

3.3.2. Molecular Basis of Solvation

We next evaluate the structure of the solvent around the oligomer to provide a

deeper insight into the solvation process. For this purpose, we compute the RDFs of the CO_2 molecules around the backbone of the CO_2 – phobic block (BCB segment). A solvation shell around 5 – 6 Å is observed for all species, with varying intensity of the peak depending on the side chain of the oligomer, as shown in Figure 3.4 For brevity and clarity, the oligomers were grouped according to the similarity of the curves; these are represented by one of their members in the figure. These groups are: [1], [2, 4, 6], [3, 8], [5, 9], [7], and [10].
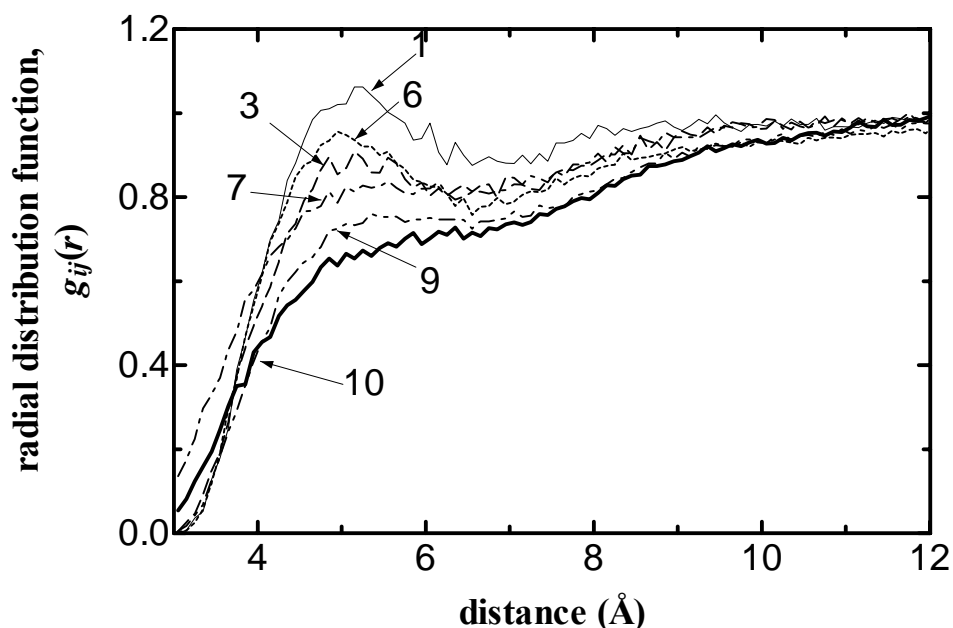
Figure 3.4. Radial distribution function between the C atoms of the CO_2 molecules and the backbone of the CO_2 – phobic segment (BCB in Figure 3.2). The oligomers that show nearly the same trend are grouped. The oligomers were grouped according to the similarity of the curves; these are represented by one of their members. These groups are: [1], [2, 4, 6], [3, 8], [5, 9], [7], and [10]

The differences in the CO_2 density near the backbone are due to (i) the available volume around the side chain, and (ii) interactions between the CO_2 molecules and the oligomer. The former forms the physical environment for CO_2 to populate around the backbone and the latter directly affects the decrease/increase in the number of CO_2 molecules near the backbone due to favorable/unfavorable interactions.

An examination of Figure 3.4 reveals that those oligomers with branched side-chains display a lower solubility in CO_2 (lowest three curves), whereas those with the smallest groups are the most soluble. In the cases where large but linear chains are

involved (6, 8), specific interactions help improve solubility. Thus, despite the larger side chain, i.e. smaller available volume to CO_2 molecules, a favourable interaction energy can enhance solvation.

In fact, to design surfactants with the desired solubility in CO_2, knowledge of the amphiphile-solvent interactions is crucial. The molecular interactions that play an essential role in solvating the amphiphile are still subject of debate[36]. Theoretical studies and NMR evidence have shown that fluorocarbons have high interaction with CO_2[61] which is further density and temperature dependent[62]. Little is known about the nature of the solvation power of CO_2 towards various solutes. In particular, even in the case of the extensively studied fluorocarbons, the dominance of van der Waals versus electrostatic interactions is the subject of discussion[63]. In this context, this study is the first attempt to describe the interactions of various functional groups with CO_2.

Oligomer	ΔE_{vdW}(kcal/mol)	ΔE_{electr}(kcal/mol)	ΔE(kcal/mol)
1	2	3	5
2	4	1	5
3	-22	0	-22
4	-33	2	-31
5	-30	-4	-34
6	-38	1	-37
7	7	3	10
8	5	8	13
9	8	5	13
10	13	3	16

Table 3.2. Estimates of nonbonded interaction energies (kcal/mol) of CO_2 – oligomer systems. ΔE_{vdW} is the van der Waals and ΔE_{electr} is the electrostatic energy contributions to the total nonbonded energy, ΔE. Energies are averaged over 0.8 ns of MD runs.

The interaction energy between CO_2 and the oligomer is estimated by equation 3.6 and the results are summarized in Table 3.2. Typical uncertainties in the energy

values are on the order of a few kilocalories. Thus, the solvent - solute interactions for chains with the smallest side groups, 1 and 2, have a small interaction energy. For larger R-groups, the oligomers having side chains 3, 4, 5, and 6 have negative overall interaction energy with CO_2, with the predominant effect coming from the van der Waals interactions. In fact, with the exception of oligomer 8, which has a slight edge for electrostatic interactions, all these oligomers have a more pronounced contribution from van der Waals interactions. Also note that oligomers 4 and 6, which have the same functionality but different size, show that chain length increases the energy of interaction in CO_2 as observed in the solubility studies of various groups[64]. For oligomer 8, the increase in the solubility despite the positive energetic contribution (see Figure 3.4) is attributed to the increased conformational freedom of the long side chain in the solvent, which in turn leads to a positive entropy of mixing large enough to overcome the unfavorable interaction energy and an overall decrease in the free energy.

3.3.3. Backbone Dynamics

The oligomers studied here are dynamic entities, which are designed to be a member in a larger array of self-organized structure. Therefore, examination of the backbone dynamics in the dilute extreme will not only let us relate to the experimentally measurable dielectic relaxation process, but it will also enable us to understand the more complex behaviour that these chains may show in the self-assembled systems.

For this purpose, the orientational time autocorrelation functions are computed for four equivalent C-F and four equivalent C-H bond vectors. The former are the two pairs of the innermost C-F vectors in the A blocks, and the latter are the two pairs of C-H vectors between the R groups of the C block. Typical curves are shown in figure 3.5, for the relaxation in oligomer 7. Stretched exponential fits are made to these curves, and the best-fit values for the relaxation time τ and the exponent β are reported in Table 3.3.

In oligomer 1, the studied C-F and C-H vectors enjoy the same environment of CO_2, due to the lack of a shielding effect from the functional groups. Although the C-F bond is somewhat stiffer than the C-H bond, both of the relaxation times are 4 ps for this oligomer. For the rest of the oligomers, the relaxation times is always shorter for the C-F vector than that for the C-H vector, in conformity with the fact that C-F bonds are stiffer and hence relax faster to their equilibrium positions. Moreover, the relaxation of

the C-H vectors is more sensitive to the identity of the functional group, which affects the immediate environment of this bond.

Oligomer	τ (ps)		β	
	C-F	C-H	C-F	C-H
1	4	4	0.9	1.
2	4	8	0.8	1.
3	7	12	0.7	0.9
4	5	14	1.	1.
5	5	16	0.8	1.
6	15	49	0.7	0.9
7	7	18	0.9	0.9
8	8	30	0.7	1.
9	9	25	0.6	1.
10	8	38	0.8	0.8

Table 3.3. Stretched exponential fits to the orientational autocorrelation function of selected C-H and C-F vectors. β is a measure of the complexity of the relaxation process, τ is the relaxation time.

In general, the characteristic time of the relaxation process mainly depends on (i) the local friction experienced by the fluctuating atoms[65, 66], (ii) the interaction energy in the medium that needs to be surmounted during the relaxation process, and (iii) the physically allowed size of the fluctuations[67, 68]. The latter may be assumed to be constant here, since we analyse the same bond vectors in all the oligomers. To understand the effect of the local environment, one might visualize trapped CO_2 molecules near the oligomer, which are compelled to interact with the backbone, resulting in a higher local friction compared to an environment where the solvent
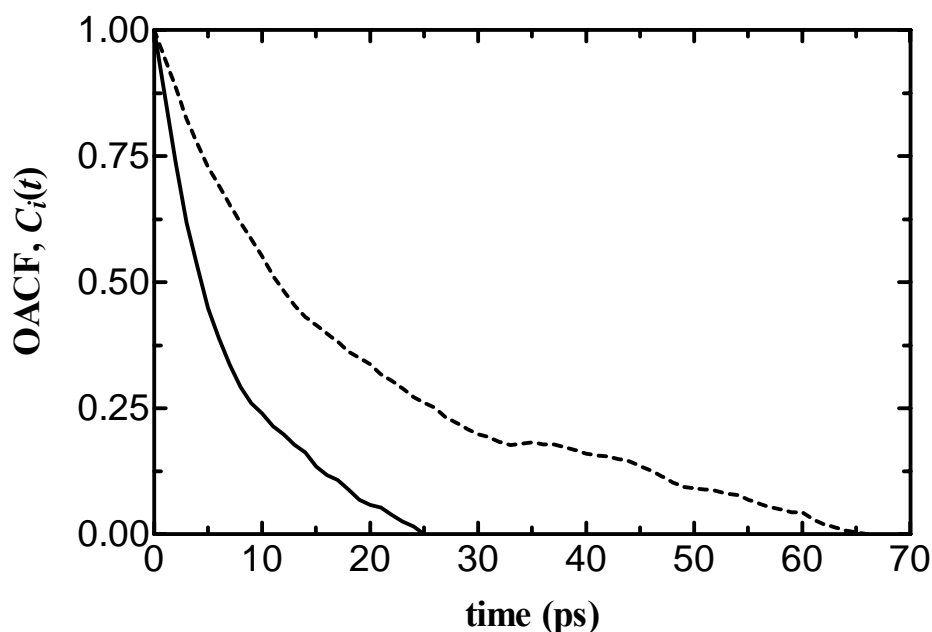
Figure 3.5. Typical orientational autocorrelation function (OACF) curves, $C_i(t) = \langle u_i(t_o) \cdot u_i(t_o+t) \rangle$, for the relaxation process of selected C–F (——) and C–H (----) bond vectors. The oligomer with side chain type 7 is shown as a representative case. The relaxation of the C-F bonds is a faster process than that of the C-H vectors due to the stiffer nature of the former, as well as the fact that they are distally located from the bulky –R groups.

molecules are free to bounce off upon random collisions with the backbone. Since the relaxation time is known to increase with the effective friction coefficient, we may conclude that the R-groups in those oligomers with the higher relaxation time provide a basis for a more persistence trapping of CO_2 molecules. The existence of a potential field that favours solvent – solute interactions (i.e. negative interaction energy), on the other hand, will slow down the dynamics of solvation (again, larger τ). A repulsive interaction will have the reverse effect. Thus, oligomer 6 provides a large void between the R-groups for solvent trapping, along with a negative interaction energy, leading to the largest relaxation time. The τ of oligomers 8, 9 and 10 are also large due to the trapping, which competes with the decreasing effect on τ of positive interaction energy. Note that, it is not the number density of CO_2 molecules around the oligomer, as pictured in Figure 3.4, that increases the local friction, but rather the trapping that is created in some of the oligomers that leads to a persistent group of CO_2 molecules near the backbone.

Finally, we examine the stretched exponent, β, which is a measure of coupling between processes occurring at distinct time scales that affect relaxation phenomenon (equation 3.9). We find that the value for the C-H bond is close to 1 in all cases, indicating that processes contributing to the relaxation of this bond are on the same order and the autocorrelation function shows simple exponential decay. On the other hand, β of C-F bond vector varies depending on the side chain, with the lowest β value for oligomer 9. Thus, the relaxation of C-F bond vectors in segment A has a more complex mechanism than that of C-H bond vectors found in segment C. Nevertheless, even a value of $\beta = 0.6$ indicates simple dynamics compared to those observed in larger molecular systems. For example, the relaxation process of similar vectors in proteins is more complicated. The relaxation of the backbone N-H vector of the Arginine 1 residue in Bovine Pancreatic Trypsin Inhibitor was analysed at various temperatures in a recent study[59]. This vector belongs to the outermost part of the protein, its local environment being the least crowded. Therefore, its relaxation should be the most decoupled from the rest of the protein, having heavy contributions from simpler processes such as those due to solvent bombardment. For this NH vector, β decreases monotonically from 0.63 at 150 K to 0.22 at 320 K. Other backbone N-H vectors in this protein have even smaller stretched exponents (unpublished results). The large stretched exponents obtained in this study, therefore, implicate that the dynamics of the single chains studied here might become more complex in a system with many interacting chains. This statement, however, needs to be verified with an additional study of several oligomers in CO_2 that display self-assembly behavior.

3.3.4. Micelle Geometry

The structures of the single chains indicate that the fluorinated block is highly stiff and have a rodlike shape in all side chain types with the end-to-end distance between the two tails are between 6 – 10 Å. The conformational flexibility of hydrocarbon backbone of the CO_2 – phobic block, on the other hand, has a similar end-to-end distance with that of the distance between the two tails, thus resulting in the open and closed structures as discussed above. In many-chain systems, these molecules are expected to assemble into inverted micelles or planar and flexible bilayers [6]. It is

interesting to note that, fluorosurfactants of these types could not form spherical or cylindrical micelles due to the bulky fluorinated tails.

4. CONCLUSIONS AND FUTURE PROSPECTS

PHU is representative of a class of bacterial polyesters, PHAs, with desirable properties such as biodegradability, biocompatibility, and environmental compatibility. However, many of these polyesters are thermally unstable and display poor mechanical properties. It may be desirable to improve their bulk or surface properties by modifying their chemical structures, cross-linking, etc. Isotactic PHU is a good candidate for such treatment, due to its long side chains that may be utilized for tuning the bulk or surface properties. Therefore, it is of utmost interest to understand the local structure of this system. In this study, the chain dimensions and conformational features of the PHU molecule are investigated using RIS calculations and MD simulations. The effects of the environment and temperature are examined in detail.

Experimental observations on PHB and our simulations of PHU exhibit similarities: (i) strong persistence for rodlike helices are observed in good solvent and the amorphous state, (ii) a sharp helix-to-coil transition is observed for both polymers in going from good to poor solvent conditions. Due to the presence of the large side chains, PHU shows Gaussian chain behavior with non-zero mean end-to-end vector. In the vacuum environment, the chain dimensions are smaller than the bulk state in both RIS and MD methods, whereas, in chloroform they are larger than the bulk value. In fact, results from the vacuum, bulk state, and chloroform simulations are representative of poor, theta, and good solvent conditions, respectively, and they reflect the expected tendency of the characteristic ratio to increase as the solvent conditions are improved.

The populations of dihedral angles change as the temperature and/or environment change, except for those of the partially double bonded ester bond. The populations of all the dihedrals at 400 K in vacuum and at 300 K in the bulk are similar. In chloroform, chain conformations converge to the structure found from the optimization of PHU in

vacuum, which also corresponds to the lowest energy structure obtained in the RIS model.

The helix size and helix persistence in the simulations is related to the quality of the solvent. In poor solvents, PHU behaves like a random coil, while in good solvents a persistent rodlike shape is observed. However, due to the lack of hydrogen bonds and the small dipole moment of the ester compared to amino groups, the helix stability is expected to be lower than that of the proteins[11]. The side chains adopt a predominantly extended conformation irrespective of the environment and the backbone conformation. This feature makes PHU an excellent candidate for a bacterial polyester whose properties may be improved upon treatment.

It has recently been proven theoretically[69], and has later been shown experimentally[70], that it is possible to obtain equilibrium properties of a system from processes carried out arbitrarily far from equilibrium. Our approach to the self-assembly behavior of amphiphiles by studying their single-chain behavior in the solvent rests upon this perspective. In this work, we study the conformational and dynamic features of amphiphiles in CO_2 at near supercritical conditions. These oligomers have segments, which tend to sequester away from the solvent, flanked on either side by CO_2 - philic fluorinated blocks. A plethora number of conformational states are accessible to a given chain. However, the intramolecular interactions of the single-chain and its local interactions with the solvent already reduce the conformational space by a very big factor. This space is further reduced as more chains interact with one-another, establishing the basis for the final molecular organization in the micelle. Thus, a detailed study of the conformations and the dynamics of these oligomers enable us to deduce some general features that may give clues on the expected behavior of the micelle

For all the amphiphiles studied here, U-shaped planar structure is attained. These have varying degrees of flapping of the fluorinated arms, depending on the identity of the attached -R groups. The fluctuations are expected to be stabilized by the presence of other chains, resulting in a truncated cone or cylindrical structure. The geometric considerations and packing constraints stated by Israelechvilli[6] proposes either planar and flexible bilayers micelles for the closed structures or inverted micelles for the open structures when they associate. It is interesting to note that, fluorosurfactants of these types due to the bulky fluorinated tails will not form spherical or cylindrical micelles.

The detailed solvation behavior of the chains, given by the amount of exposure of the backbone to the solvent molecules (Fig. 3.3), depends on the character of the -R groups in the middle of the chain. In fact, the delicate balance between the available volume around the side chain, and the specific interactions between CO_2 molecules and the oligomer dictate the final amount of solubility. The origin of energy of solvation is investigated in detail. van der Waals interactions are found to dominate over electrostatic interactions, unless there is a strong partial charge on the side-chain atoms.

The dynamics of the chains, measured by the relaxation time of selected bond vectors, depend on the local friction experienced by the atoms and the interaction energy that needs to be surmounted during the relaxation process. In particular, the larger -R groups (cases 6, 8, 9, and 10) are found to create a trapping effect on the solvent molecules, leading to an increase in local friction and an overall retardation of relaxation phenomena. In general, the relaxation phenomena of the investigated bond vectors are found to obey a simple exponential decay, indicating a lack of coupling between processes occurring at distinct time scales. A complication of these relaxation processes is expected for self-assembled systems.

Here, we have performed a detailed analysis of the single-chain behavior of oligomers that tend to self-assemble into micellar structures. In future work, we will study the behavior of many-chain systems. In particular, we will follow the evolution of the systems towards the micellar organization, and we will study their conformational properties and dynamic behavior in the assembly. Understanding the single-chain behavior is crucial for distilling the factors that emerge solely due to the organized structure. Our ultimate goal is to deduce phenomena underlying the self-assembly behavior of molecular systems

.

REFERENCES

1. Bovey, F.A. and F.H. Winslow, *Macromolecules, An Introduction to Polymer Science*. 1992, New York: Academic Press, Inc.

2. Flory, P.J., *Principles of Polymer Chemistry*. 1953, Itacha and London: Cornell University Press.

3. Haile, J.M., *Molecular Dynamics Simulation*. 1997, New York: John Wiley and Sons, Inc.

4. Leach, A.R., *Molecular Modelling Principles and Applications*. 1998, England: Longman.

5. Baysal, C., *Efficient Computational Models and Methods for Investigating Local Polymer Dynamics*, in *Chemical Engineering*. 1996, Bogazici University: Istanbul.

6. Israelachvili, J., *Intermolecular and Surface Forces, p381*. 1997, London: Academic Press.

7. Cornibert, J. and R.H. Marchessault, *Physical Properties of Poly(β–hydroxybutyrate)*. J. Mol. Biol., 1972. **71**: p. 735-756.

8. Avella, M., E. Martuscelli, and M. Raimo, *Properties of Blends and Composites Based on Poly(3-hydroxy butyrate) (PHB) and Poly(3-hydroxybutyrate-hydroxyvalerate) (PHBV) Copolymers*. J. Mat. Sci., 2000(35): p. 523-545.

9. Pazur, R.J., et al., *Molecular Modelling of Helical and Extended-chain Polyhydroxybutyrates and Polytetramethylene Succinate*. Polymer, 1998. **39**(14): p. 3065.

10. Brückner, A., et al., *Physical Properties of Poly(hydroxybutyrate)*. Macromolecules, 1988. **21**: p. 967.

11. Marchessault, R.H., K. Okamura, and C.J. Su, *Physical Properties of Poly(beta-hydroxy butyrate) II. Conformational Aspects in Solution*. Macromolecules, 1970. **3**(6): p. 735-740.

12. Miyaki, Y., et al., *Solution Properties of Poly(β–hydroxy butyrate).* Macromolecules, 1977. **10**(1356).

13. Huglin, M.B. and M. Radwan, *Unperturbed Dimensions of Poly(3-hydroxybutyrate) in Single and Binary Solvents.* Polymer, 1991. **32**(7): p. 1293.

14. Beaucage, G., et al., *Persistence Length of Isotactic Poly(hydroxybutyrate).* Macromolecules, 1997. **30**: p. 4158-4162.

15. Flory, P.J., *Statistical Mechanics of Chain Molecules.* 1969, New York: Wiley.

16. Sun, H., *Forcefield for Computation of Conformational Energies, Structures, and Vibrational Frequencies of Aromatic Polyesters.* J. Comput. Chem., 1994. **15**(752).

17. Sun, H., *Ab-initio Calculations and Forcefiled Development for Computer-Simulation of Polysilanes.* Macromolecules, 1995. **28**: p. 701.

18. Andersen, H.C., *Molecular Dynamics Simulations at Constant Pressure and/or Temperature.* J. Chem. Phys., 1980(72): p. 2384.

19. Andersen, H.C., *Rattle: A 'velocity' Version of the Shake Algorithm for Molecular Dynamics Calculations.* J. Comput. Phys., 1983. **52**: p. 24-34.

20. Allen, M.P. and D.J. Tildesley, *Computer Simulation of Liquids.* 1987, Oxford: Oxford University Press.

21. Nosé, S., *A Molecular Dynamics Method for Simulations in The Canonical Ensemble.* Mol. Phys., 1984. **50**: p. 255-268.

22. Hedenqvist, M.S., R. Bharadwaj, and R.H. Boyd, *Molecular Dynamics Simulation of Amorphous Poly(ethyleneterephthalate).* Macromolecules, 1998. **31**: p. 1556-1564.

23. McHugh, M.A. and V.J. Krukonis, *Supercritical Fluids Extraction: Principles and Practice.* Vol. 2. 1993, Stoneham: Butterworth-Heinman.

24. Folk, S.L., J.M. DeSimone, and E.T. Samulski, *Cationic Poly(dimethylsiloxane) Surfactants: Synthesis, Characterization, and Aggregation Behavior in Dense Carbon Dioxide, Fluorinated, and Silicon-containing Solvents.* Polymer Preprints, 2001. **42 (1)**: p. 231.

25. Sarbu, T., T. Styranec, and E.J. Beckman, *Non-fluorous Polymers with Very High Solubility in Supercritical CO_2 Down to Low Pressures.* Nature, 2000. **405**: p. 165.

26. Maury, E.E., et al., *Graft Copolymer Surfactants for Supercritical Carbon Dioxide Applications.* Polymer Preprints, 1993. **34**: p. 664.

27. DeSimone, J.M., et al., *Dispersion Polymerizations in Supercritical Carbon Dioxide.* Science, 1994. **265**: p. 365.

28.   McClain, J.B., et al., *Design of Nonionic Surfactants for Supercritical Carbon Dioxide.* Science, 1996. **274**: p. 2049.

29.   Consani, K.A. and D.R. Smith, *Observations on the Solubility of Surfactants and Related Molecules in Carbon Dioxide at 50°C.* J. Supercritical Fluids, 1990. **3**: p. 51.

30.   Jönsson, B., O. Edholm, and O. Teleman, *Molecular Dynamics Simulations of a Sodium Octanoate Micelle in Aqueous Solution.* J. Chem. Phys, 1986. **85**(4): p. 2259-2271.

31.   Tieleman, D.P., D. Spoel van der, and H.J.C. Berendsen, *Molecular Dynamics Simulation of Dodecylphosphocholine Micelles at Three Different Aggregate Sizes: Micellar Structure and Chain Relaxation.* J. Phys. Chem. B, 2000. **104**: p. 6380-6388.

32.   Smit, B., et al., *Computer Simulations of Water/Oil Interface in the Presence of Micelles.* Nature, 1990. **348**: p. 624-626.

33.   Karaborni, S., et al., *Simulating the Self-Assemly of Gemini (Dimeric) Surfactants.* Science, 1994. **266**: p. 254-256.

34.   Karaborni, S. and J.P. O'Connell, *Molecular Dynamics Simulations of Model Micelles. 4. Effects of Chain Length and Head Group Characteristics.* J. Phys. Chem., 1990. **94**: p. 2624-2631.

35.   Johntson, K.P., et al., *Water-in-Carbon Dioxide Microemulsions: An Environment for Hydrophiles Including Proteins.* Science, 1996. **271**: p. 624.

36.   Lisal, M., et al., *Self-assembl of Surfactants in a Supercritical Solvent from Lattice Monte Carlo Simulations.* J. Chem. Phys., 2002. **116**(3): p. 1171-1184.

37.   Nagarajan, R., *Modeling Solution Entropy in the Theory of Micellization.* Colloids and Surfaces A, 1993. **71**: p. 39-64.

38.   Care, C.M. and T. Dalby, *Packing Entropy in Micelle Self-Assembly.* Europhys. Lett., 1999. **45**(1): p. 38-44.

39.   Haliloglu, T. and W.L. Mattice, *The Roles of chi and n on the Dynamics of the Exchange of Chains Between Micelles Formed by Diblock Copolymers in Selective Solvents at Concentrations Slightly Above the Critical Micelle Concentration.* Comput. Polym. Sci., 1995. **5**(1-2): p. 65-70.

40.   Smit, B., et al., *Computer Simulations of Surfactant Self-Assembly.* Langmuir, 1993. **9**: p. 9-11.

41.   Bast, T. and R. Hentschke, *Molecular Dynamics Simulation of a Micellar system: 2,3,6,7,10,11-hexakis(1,4,7-trioxaoctyl)triphenylene in Water.* J. Phys. Chem., 1996. **100**: p. 12162-12171.

42. Maillet, J.-B., V. Lachet, and P.V. Coveney, *Large Scale Molecular Dynamics Simulation of Self-assembly Processes in Short and Long Chain Cationic Surfactants.* Phys. Chem. Chem. Phys., 1999. **1**(23): p. 5277-5290.

43. Fodi, B. and R. Hentschke, *Simulated Phase Behavior of Model Surfactant Solutions.* Langmuir, 2000. **16**(4): p. 1626-1633.

44. Salaniwal, S., et al., *Self-Assembly of Reverse Micelles in Water/Surfactant/Carbondioxide Systems by Molecular Simulation.* Langmuir, 1999. **15**: p. 5188-5192.

45. Salaniwal, S., et al., *Molecular Dynamics Simulation of Reverse Micelles in Supercritical Carbondioxide.* Ind. Eng. Chem. Res., 2000. **39**: p. 4543-4554.

46. Salaniwal, S., et al., *Molecular Simulation of a Dichain Surfactant/Water/Carbondioxide System. 2.Self-Assembly and Aggregation.* Langmuir, 2001. **17**: p. 1784-1792.

47. Eastoe, J., et al., *Droplet Structure in a Water-in-CO$_2$ Microemulsion.* Langmuir, 1996. **12**: p. 1423-1424.

48. Baysal, C., B. Erman, and B. Chu, *Conformational Features of Poly(1,1dihydroperfluorooctyl acrylate) and Poly(vinyl acetate) Diblock Copolymers in Supercritical Carbon Dioxide.* J. Chem. Phys., 2001. **114**(12): p. 5444-5449.

49. Zhou, S. and B. Chu, *Laser Light Scattering Study of Pressure-Induced Micellization of a Diblock Copolymer of Poly(1,1-dihydroperfluorooctylacrylate) and Poly(vinyl acetate) in Supercritical Carbon Dioxide.* Macromolecules, 1998. **31**: p. 5300.

50. Zhou, S. and B. Chu, *Self-Assembly Behavior of a Diblock Copolymer of (1,1-dihydroperfluorooctyl acrylate) and Poly(vinyl acetate) in Supercritical Carbon Dioxide.* Macromolecules, 1998. **31**: p. 5300-5308.

51. Li-Zhi, L., et al., *Synchrotron SAXS and Laser Light Scattering Studies of Agregation Behavior of Poly(1,1-dihydroperfluorooctyl acrylate-b-vinyl acetate) Diblock Copolymer in Supercritical Carbon Dioxide.* Macromolecules, 1999. **32**: p. 5836-5845.

52. Dauber-Osguthorpe, P., et al., *Structure and Energetics of Ligand Binding to Proteins: E. coli Dihydrofolate Reductase-Trimethoprim, a Drug-Receptor System.* Proteins, 1988. **4**(31).

53. Maple, J.R., et al., *Derivation of Class II Force Fields. I. Methodology and Quantum Force Field for the Alkyl Functional Group and Alkane Molecules.* J. Comput. Chem., 1994. **15**(162).

54. Golub, G.H. and G.H. van Loan, *Matrix Computations.* 1989: Johns Hopkins University Press.

55.   McQuarrie, D.A., *Statistical Mechanics*. 1976, New York: Harper and Row.

56.   Williams, G. and D.C. Watts, *Non-symmetrical Dielectric Relaxation Behavior Arising from a Simple Empirical Decay Function.* Trans. Faraday. Soc., 1970. **66**: p. 80-85.

57.   Haliloglu, T., I. Bahar, and B. Erman, *Orientational and Conformational Correlations in Deformed Polymer Chains with Fixed end-to-end Seperation: A Brownian Dynamics Simulation Study.* J. Chem. Phys., 1992. **97**: p. 4428-4437.

58.   Deschenes, L.A. and D.A. Vanden Bout, *Single-Molecule Studies of Heterogeneous Dynamics in Polymer Melts Near the Glass Transition.* Science, 2001. **292**: p. 255-258.

59.   Baysal, C. and A.R. Atilgan, *Relaxation Kinetics and the Glassiness of Proteins: The Case of Bovine Pancreatic Trypsin Inhibitor.* Biophys. J., 2002. **83**: p. 699-705.

60.   Kohlrausch, R., *Theorie des Elektrischen Rückstandes in der Leidener Flasche.* Ann. Phys. Chem. (Leipzig), 1974. **91**: p. 179-214.

61.   Cece, A., et al., *Molecular Modelling Approach for Contrasting the Interactions of Ethane and Hexafluoroethane with Carbondioxide.* J. Phys. Chem, 1996. **100**: p. 7435-7439.

62.   Dardin, A., J.M. DeSimone, and E.T. Samulski, *Fluorocarbons Disolved in Supercritical Carbondioxide. NMR Evidence for Specific Solute-Solvent Interactions.* J. Phys. Chem. B, 1998. **102**: p. 1775-1780.

63.   Lee, C.T., et al., *Water-in-Carbon Dioxide Emulsions: Formation and Stability.* Langmuir, 1999. **15**: p. 6781-6791.

64.   Kirby, C.F. and M.A. McHugh, *Phase Behaviour of Polymers in Supercritical Fluid Solvents.* Chem. Rev., 1996. **99**: p. 565-602 and references therein.

65.   de Gennes, P.-G., *Origin of Internal Viscosities in Dilute Polymer Solutions.* J. Chem. Phys., 1977. **66**: p. 5825-5826.

66.   de Gennes, P.-G., *Scaling Concepts in Polymer Physics.* 1979, Cornell University Press: Ithaca. p. 198.

67.   Bahar, I., B. Erman, and L. Monnnerie, *Effect of Surrounding Mediumon Intermolecular Conformational Changes in Probe Molecules.* Macromolecules, 1990. **23**: p. 3805-3811.

68.   Baysal, C., et al., *Local Dynamics of Bulk Polybutadienes of Various Microstructures: Comparison of Theory with Experiment.* Macromolecules, 1997. **30**: p. 2058-2066.

69.   Liphardt, J., et al., *Equilibrium Information from Nonequilibrium Measurements in an Experimental Test of Jarzynski's Equality.* Science, 2002. **296**: p. 1832-1835.

70.   Jarzynski, C., *Nonequilibrium Equality for Free Energy Differences.* Phys. Rev. Lett., 1997. **78**: p. 2690.